nature portfolio

Peer Review File

Decoupling fast hydrogen oxidation reaction on a tandem electrocatalyst

Corresponding Author: Professor Wenping Sun

This file contains all reviewer reports in order by version, followed by all author rebuttals in order by version.

Attachments originally included by the reviewers as part of their assessment can be found at the end of this file.

Version 0:

Reviewer comments:

Reviewer #1

(Remarks to the Author)
In this study, a Ru-based tandem HOR catalyst was designed, with Ru nanoclusters (NCs) decorated with Pt single atoms. The experimental and theoretical studies suggest that the H2 dissociation step occurs at Ru sites, and then the produced H species migrate to Pt sites followed by the desorption of H+. The key here is that the strong Ru-H interaction promotes the H2 dissociation step, while the optimum Pt-H interaction ensures the fast desorption process, thereby substantially enhancing the HOR kinetics. I would like to recommend its acceptance for publication after the following revisions:
1.In Figure 2, how to explain the difference in the limiting diffusion current density in the LSV curves of Pt/C and Pt1 - Ru/C?
2.In Figure S17, it can be clearly observed from the image that the HOR performance of Pt1 - Ru/C - 2 is inferior to that of Pt1 - Ru/C. Has it been considered that there might exist a Pt1 - Ru/C material with a higher MA at a platinum single - atom density ratio between that of Pt1 - Ru/C and Pt1 - Ru/C - 2?
3.Is it possible to confirm the EXAFS signal of Pt-Ru coordination but not Pt-Pt coordination in Pt1-Ru/C?
4.The CO stripping curves are suggested to be added to corroborate the speculation regarding the CO poisoning resistance of the Pt1 - Ru/C material.
5.The article lacks tests on the stability of the catalyst. Please supplement the ADT data of the material or the stability test data in the PEMFC.
6.In Figure 4a, the change in the desorption peak potential is not clear. An arrow can be added to illustrate the trend of the peak potential change. According to Fig. 4d, what are the reasons for elevated limiting current densities?
7.In Figure 5d, the names of the elements represented by different spheres should be marked.
8.Please elaborate on why the potential for comparing the KIE of the HOR is around 0.3 - 0.5 V. Explain why the 0.3 - 0.5 V range represents the mass transfer region. Is it possible to narrow or expand this mass transfer region?
9.According to Fig. S18, whether the Pt1/C catalyst does not have catalytic activity can be attributed to the unsuccessful loading of Pt on C.
10.Stability is a key indicator for evaluating the practical application potential of catalysts. Does Pt1-Ru/C have excellent catalytic stability and structural stability?
11.There are many grammar mistakes in this manuscript and the authors should check the manuscript.

Reviewer #2

(Remarks to the Author)
The authors report an interesting Pt-Ru/C catalyst for the hydrogen oxidation reaction (HOR), attributing the enhanced performance to the hydrogen spillover effect from Ru to Pt. This catalyst achieves a peak power density of 1.91 W cm^{-2} at an ultralow loading of 5 μgPGM cm^{-2}, meeting the DOE target. While the work presents promising results, I disagree with some of the explanations, and several aspects remain unclear or contain mistakes. Therefore, I believe a major revision is necessary.

1.It is unclear how the Pt-Ru catalyst is defined. Are Pt and Ru forming a composite or an alloy? Is Pt located on the surface of Ru clusters, or is there surface exchange between Pt and Ru to form an alloy structure? This distinction is crucial, especially for accurately constructing the model for DFT calculations. Based on the current characterization and analysis provided, the structure remains ambiguous. Please clarify with additional evidence or characterization.

2.While the catalyst demonstrates impressive peak power density, it is essential to present its stability performance. How does the catalyst perform over extended operation? Additionally, it would be valuable to compare your results with recent literature, focusing on peak power density, mass activity, and long-term stability.
3.Did the authors investigate the effect of varying Pt and Ru ratios in the catalyst? How do different weight percentages influence performance and hydrogen spillover? For instance, would increasing the Pt content improve the catalyst's activity? Including such data would strengthen the conclusions.
4.In Figure 3a–c, is there evidence of Ru dissolution during oxidation? If Ru dissolves, this could lead to Pt detachment. If this occurs, how is the sustained performance in Figure 3c explained? Please provide further discussion or experimental verification.
5.I agree that the KIE experiment supports the observation of faster kinetics for the HOR. However, I did not find a clear explanation of how this experiment specifically validates the proposed hydrogen spillover mechanism. Please elaborate on how the experimental results validate the spillover process or consider conducting additional experiments to substantiate this claim.
Other non-scientific points
6.Figure 2 is missing sub-labels (a, b, c, d). Please revise to ensure clarity and consistency.
7.In the supporting information, the notation in catalyst names, such as "Pt1-Ru/C-0.5-A" and "Pt1-Ru/C-2-A," is unclear. What do the numbers "1," "-0.5," and "-2" represent? Providing a clear explanation of this naming convention would help readers better understand the catalyst variations.
8.The manuscript lacks details on the EXAFS fitting procedure. Please describe the fitting process in detail, including fitting parameters, reference models, and error analysis.

Reviewer #3

(Remarks to the Author)
This work, using Pt1-Ru/C catalyst as a model catalyst, demonstrates a tandem electrocatalysis to decouple the HOR process, and shows a high-performance Ru-based tandem HOR electrocatalyst for PEMFCs. The reaction mechanism is studies through both experimental and theoretical methods. The following concerns are still need to be addressed.
1. In Figures 1b and S6d, high-contrast bright spots are distinctly distributed not only on the Pt_1Ru nanoparticles but also on the carbon support. These metallic sites on the support may also exhibit catalytic activity during reactions. The authors should further elucidate the catalyst structure and investigate whether synergistic effects exist between Pt/Ru single atoms on the support and the Pt_1Ru nanoparticles.
2. On Page 4, Lines 101–102, "Pt exists in the form of Cl-coordinated single atom in Pt1-Ru/C (Figure 1d-e and Figure S11), …" was mentioned. Following on from the previous question, the coordination of Cl may only be on the Pt1/C sites, while the coordination of Pt on the Pt1Ru nanoparticles may be different.
3. For the XAS analysis, typical M-M coordination, i.e. Pt-Ru, should also exist in the Pt1Ru particles but missing in the provided data analysis. Please explain or recheck it.
4. The statement in lines 110-111 claims "Pt is further reduced and converted into oxygen-coordinated single atoms during the HOR process". However, there is a causal link between this structural evolution and the enhanced HOR performance. To strengthen the mechanistic rigor, please discuss the structure-activity relationship between Pt-O coordination and HOR.
5. The use of mass-normalized current density at 50 mV overpotential (Figure S17d) to evaluate and compare the mass activity of catalysts in this study appears insufficiently rigorous and accurate. As evident from Figure 2a, the current density of both Pt1-Ru/C and Pt/C at 50 mV overpotential have approached (or even reached) the limiting diffusion current density (jl). This strongly suggests that the reported current density at 50 mV is dominated by H_2 mass transport rather than intrinsic kinetics, rendering it unsuitable for evaluating true mass activity. In HOR research, the universally accepted standard metrics for mass activity are the following: (1) Mass-normalized exchange current density (j0,m) derived from kinetic analysis (e.g., Tafel fitting in the low-overpotential region); (2) Mass-normalized kinetic current density (jk,m) corrected for mass transport limitations at a defined overpotential interval (10~50 mV), typically via rotating disk electrode (RDE) measurements. I suggest recalculating the mass activity using j0,m and jk,m to enable a rigorous comparison.
6. Regarding the hydrogen spillover mechanism, the authors should supplement more experiments (such as in-situ impedance tests) to provide evidence. The difference in *H adsorption energy between Ru and Pt from theoretical calculations is insufficient to fully demonstrate the occurrence of hydrogen spillover.
7. For PEMFCs, the CO poisoning resistance of anode hydrogen oxidation reaction (HOR) catalysts is a critical metric for practical device applications. The authors should supplement the study with experiments (e.g., CO stripping voltammetry or tolerance tests under CO-containing atmospheres) to demonstrate the anti-CO poisoning performance of the catalysts.
8. For PEMFCs test, the absence of long-term durability significantly limits its practical relevance. For catalyst benchmarking in fuel cells, stability under realistic operating conditions is a critical metric for industrial applicability. I suggest the authors to conduct stability measures.

Reviewer #4

(Remarks to the Author)
This research developed a tandem catalyst composed of ruthenium nanoclusters decorated with platinum single atoms. Additionally, a unique reaction mechanism involving hydrogen spillover was demonstrated through electrochemical tests, operando analysis, and DFT calculations. Especially, the originality of this paper lies in reducing the cost of the PEMFC single cell by drastically minimizing the anode platinum usage. However, additional experiments seem necessary to further explain the performance improvement and enhance its practical applicability. Therefore, this paper requires minor revision for publication in Nature Communications.

Reviewer #5

(Remarks to the Author)
The manuscirpt presents a Pt1-Ru catalyst for efficient HER and HOR. A tandem mehcanism in which hydrogen splillover from Ru to Pt site is proposed. The authors performed passivation, KIE, FTIR, and DFT calculations to support their hypothesis. Although the performance of the catalyst is impressive, the active site assignments are not consistent throughout the study, which renders the mechanistic study untrustworthy. The detailed comments are listed below. Based on these inconsistencies presented in the study, I do not recommend the manuscript for publication in Nat. Commun. in its current form.

1. The EXAFS in Figure 1d and fitting results seem to support that Pt has O/Cl coordinations and its oxidation state is 2+ or 4+. However, in the Pt single atom is modeled with Pt adatom on Ru surface, which has no ligand protection and should be of oxidation state 0. This inconsistency with EXAFS characterization results and DFT model decrease the reliability of the proposed tandem mechanism.

2. The working conditions is not taken into account for mechanism proposal and the active site is not clear for HOR/HER. The authors mentioned that Ru starts to be oxidized at 0.1 V, so in the HOR conditions, are Ru metallic or bounded with OH and O? What are the influences of Ru oxidation state on H2 dissociation reaction? Does it influence the H spillover to Pt? I think these are important points that needed to be further elucidated. The same question also needed to be answered for HER.

3. In HER conditions, Pt1-Ru catalysts is supposed to be reduced. Does it lead to Pt aggregation because of the ligand removal? What the the form of Pt and Ru in HER conditions?

4. The noise to signal ratio of the FTIR data in Figure 5 is really bad. I don't think it gives out reliable support for the proposed mechanism. And, H* binds to the hollow site on Ru instead of top site.

5. in DFT calculations of hydrogen dissolution, I found that the H2 dissociates into a surface H* and a H in vacuum as seen in Figure 6b. The model is not realistic.

6. in Figure 1d caption, it should be EXAFS not XANES.

Version 1:

Reviewer comments:

Reviewer #1

(Remarks to the Author)
The authors have answered all of the questions. It can be considered as a publication in the present form.

Reviewer #2

(Remarks to the Author)
The authors have responded to all of my comments. I am satisfied with the current version and believe it is suitable for publication.

Reviewer #3

(Remarks to the Author)
The authors have addressed the points and concerns raised by the reviewers, and the revised manuscript appears suitable for publication.

Reviewer #4

(Remarks to the Author)
The authors have adequately addressed all reviewer concerns. In response to my primary comment, they provided a clear explanation regarding the hydrogen spillover effect and its saturation behavior, supporting their claim with comparative electrochemical data (Figure R33). They convincingly argue that the slightly lower mass-normalized activity of Pt_1-Ru/C-2 stems from the excess Pt atoms not contributing to spillover interactions due to surface saturation. This mechanistic rationale is supported by both experimental trends and structural considerations.
Furthermore, the authors responded rigorously to the EXAFS coordination concerns, incorporating continuous Cauchy wavelet transform (CCWT) analysis to clarify the emergence of Pt–Ru bonding post-activation. The identification of metal–metal coordination at ~2.65 Å and corresponding k-space shifts substantiates their interpretation. Additionally, their explanation of oxidation state changes via electron transfer from Ru to $PtCl_6^{2-}$ is consistent with the spectroscopic data. Finally, they supplemented the manuscript with a 40-hour PEMFC durability test under H_2–air conditions (Figure R36), demonstrating minimal degradation and reinforcing the catalyst's practical viability. Overall, the revised manuscript

demonstrates a high level of technical rigor, originality, and relevance to the field of low-PGM PEMFCs. I consider it suitable for publication in Nature Communications after minor revision.

Reviewer #5

(Remarks to the Author)
The computational model has been improved in the revised manuscript. However, the Figure 6 in the revised manuscript seems still not supporting the H spillover mechanism since uphill free energy lanscape for H* migrating from Ru to Pt sites are obtained. So basically, H* spillover is not thermodynamically supported. The author needs to futher elucidate why Ru could accelerate the HOR. To the best of my knowledge, Pt itself could readily dissociate H2 into H*, would Ru be neccesary to facilitate H-H bond breaking? And, as H* adsorbed strongly on Ru, it is expected that H* may not easily migrate to Pt. These points need to be further elucidated.

Version 2:

Reviewer comments:

Reviewer #5

(Remarks to the Author)
The author have addressed all my concerns. The manuscript could be accepted in Nat. Commun. by its current form.

Responses to Reviewers

First of all, we sincerely thank you for your constructive comments and suggestions, which have improved the clarity of our manuscript. We have read through the referees' comments and revised the manuscript carefully. Point by point responses are shown below.

Reviewer #1: In this study, a Ru-based tandem HOR catalyst was designed, with Ru nanoclusters (NCs) decorated with Pt single atoms. The experimental and theoretical studies suggest that the H_2 dissociation step occurs at Ru sites, and then the produced H species migrate to Pt sites followed by the desorption of H^+. The key here is that the strong Ru-H interaction promotes the H_2 dissociation step, while the optimum Pt-H interaction ensures the fast desorption process, thereby substantially enhancing the HOR kinetics. I would like to recommend its acceptance for publication after the following revisions:

Comment 1: In Figure 2, how to explain the difference in the limiting diffusion current density in the LSV curves of Pt/C and Pt1-Ru/C?

Response to Comment 1: In the rotating disk electrode (RDE) system, the limiting current density expression for the HOR is given by:

$$j_L = 0.62nFD^{2/3}\omega^{1/2}\gamma^{-1/6}C$$

n = number of electrons transferred

F = Faraday constant (96485 C/mol)

D = diffusion coefficient of hydrogen (cm^2/s)

C = bulk concentration of hydrogen (mol/cm^3)

ω = angular rotation rate of the electrode (rad/s)

v = kinematic viscosity of the solution (cm^2/s)

Here, the F, C, ω, and v are fixed constants, and the electron transfer numbers (n) were determined to be 1.98 and 1.97 for Pt1-Ru/C and Pt1/C, respectively (**Figure R1**). Therefore, the difference in the limiting diffusion current density between Pt/C and Pt1-Ru/C should be ascribed to the different diffusion coefficient (D).

Meanwhile, the *in situ* electrochemical impedance spectroscopy (EIS) investigations were carried out to investigate the H_2 mass transfer behavior. The Nyquist plots were simulated by

a double-parallel equivalent circuit model (Figures S37-38 and Table S7 in the revised Supplementary Information). The second parallel component R_2 represents the H_2 mass transfer resistance from solution to catalyst surface in the HOR (*Small* 2024, 20, 2308053, *ACS Meas. Sci. Au.* 2023, 3, 162). As displayed in **Figure R2** (Figure S39 in the revised Supplementary Information), Pt/C catalyst displays a higher H_2 mass transfer resistance than Pt1-Ru/C catalyst in the whole HOR overpotential region. These results support that it is the different hydrogen diffusion behavior that leads to the different limiting current densities.

Also, H_2 diffusion is sufficiently rapid in practical PEMFCs and does not impose significant limitations on the HOR.

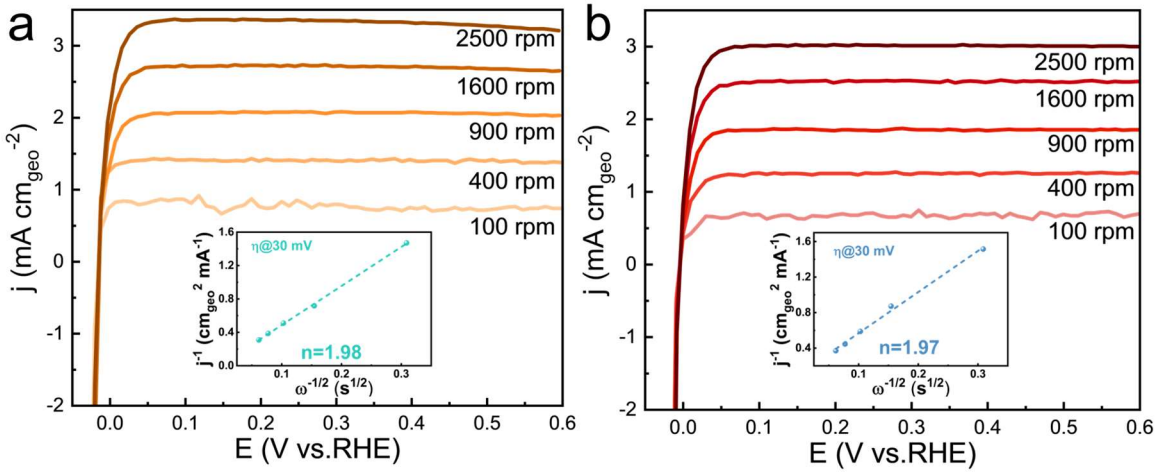

Figure R1. LSV curves of Pt1-Ru/C (a) and Pt/C (b) at various rotation rates, and the inset shows the Koutecky–Levich plot at an overpotential of 30 mV.

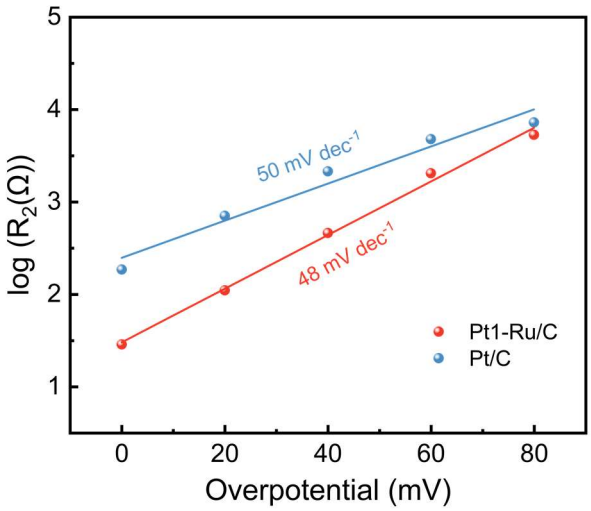

Figure R2. EIS-derived Tafel plots of different catalysts.

Comment 2: In Figure S17, it can be clearly observed from the image that the HOR performance of Pt1-Ru/C-2 is inferior to that of Pt1-Ru/C. Has it been considered that there might exist a Pt1-Ru/C material with a higher MA at a platinum single-atom density ratio between that of Pt1-Ru/C and Pt1-Ru/C-2?

Response to Comment 2: We have further synthesized a series of Pt1-Ru/C samples with varying Pt loadings, namely Pt1-Ru/C-0.75, Pt1-Ru/C-1.25, Pt1-Ru/C-1.5, and Pt1-Ru/C-1.75, which were synthesized via the same method with the addition of 45, 75, 90, and 105 μL of 0.01 M H_2PtCl_6 solution, respectively. The Ru and Pt elemental contents in these samples were determined using inductively coupled plasma mass spectrometry (ICP-MS) in **Table R1**.

Table R1. Mass percent of Ru and Pt in different samples determined by ICP.

mass percent	Ru	Pt
Pt1-Ru/C-0.75	1.23%	0.12%
Pt1-Ru/C-1.25	1.32%	0.16%
Pt1-Ru/C-1.5	1.14%	0.20%
Pt1-Ru/C-1.75	1.31%	0.21%

The HOR activities and mass activities (MA) are displayed in **Figure R3**. The Pt1-Ru/C sample is still the best among these catalysts.

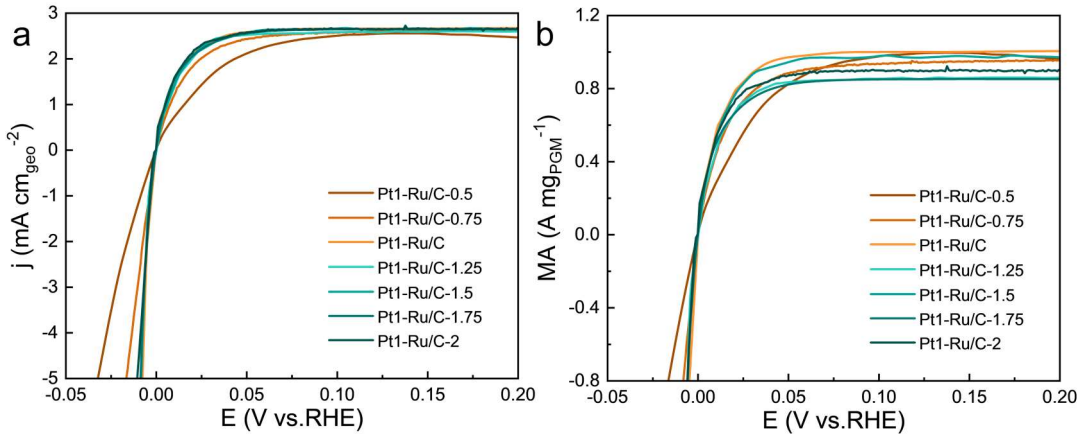

Figure R3. (a) HOR and (b) mass-normalized HOR polarization curves of different catalysts in H_2-saturated 0.5 M H_2SO_4 with a scanning rate of 5 mV s^{-1} at 1,600 rpm.

Comment 3: Is it possible to confirm the EXAFS signal of Pt-Ru coordination but not Pt-Pt coordination in Pt1-Ru/C?

Response to Comment 3: The EXAFS signal in Pt1-Ru/C can be confirmed as the Pt-Ru coordination base on the continuous Cauchy wavelet transform (CCWT) analyses (**Figure R3**). It has been reported that the downshift of a signal in k-space indicated the presence of lighter elements in the coordination shell (*Nat Energy,* 2021, 6, 1144–1153). As depicted in **Figure R3a-b** (Figures S17-18 in the revised Supplementary Information), a metal-metal coordination in Pt1-Ru/C-A can be observed at 2.65 Å in R-space and 7.0 $Å^{-1}$ in k-space, which is apparently smaller than that of Pt-Pt bond in Pt foil (9.8 $Å^{-1}$ in k-space). Therefore, the EXAFS signal in Pt1-Ru/C can be confirmed as the Pt-Ru coordination.

Relevant discussions have been provided on pages 4-5 in the revised manuscript.

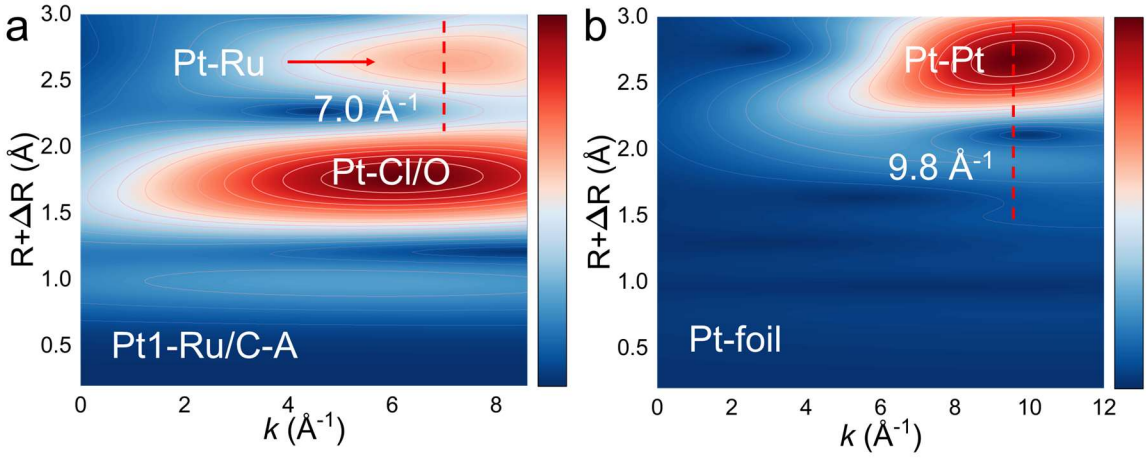

Figure R3. The corresponding Cauchy Wavelet Transform (CCWT) for the k^3-weighted EXAFS signals at the Pt1-Ru/C-A (a) and Pt-foil (b).

Comment 4: The CO stripping curves are suggested to be added to corroborate the speculation regarding the CO poisoning resistance of the Pt1-Ru/C material.

Response to Comment 4: The CO stripping curves have been provided in Figure S30 in the revised Supplementary Information (**Figure R4**). The Pt1-Ru/C catalyst exhibits a significantly lower onset potential for CO stripping compared with Ru/C and Pt/C catalysts, which is consistent with its superior CO tolerance. Relevant discussions have been provided on page 7 in the revised manuscript.

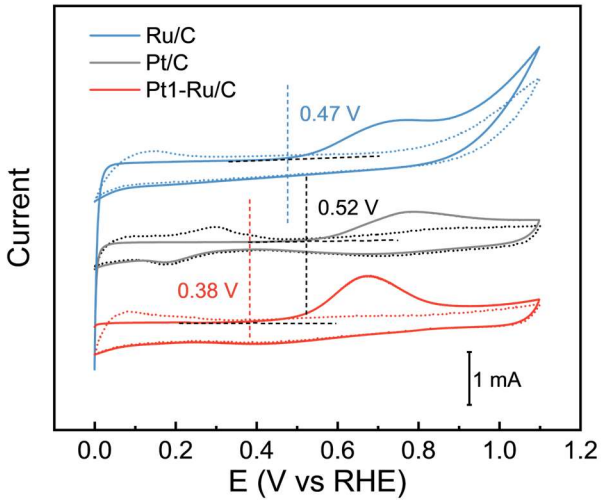

Figure R4. CO-stripping measurements for Ru/C, Pt/C, and Pt1-Ru/C.

Comment 5: The article lacks tests on the stability of the catalyst. Please supplement the ADT data of the material or the stability test data in the PEMFC.

Response to Comment 5: We have tested the stability of the catalyst including an ADT of the catalyst using RDE and a 40-h test in real PEMFC. The results and the corresponding discussions have been updated on the pages 6-7 in the revised manuscript.

First, we examined the HOR stability of Pt1-Ru/C by an accelerated durability test (ADT) and a chronoamperometry response test, as depicted in **Figures R5-6** (Figures S26-28 in the revised Supplementary Information). After 1000, 3000 and 5000 cyclic voltammetry (CV) cycles, the overpotential at 1 mA cm^{-2} increases by only about 1, 2 and 4 mV, respectively (**Figure R5a**). The result demonstrates evidently higher stability of Pt1-Ru/C than Pt/C (**Figure R5b**). Additionally, as shown in **Figure R6**, the Pt1-Ru/C catalyst displays excellent durability without obvious decay for 70 h operation at an overpotential of 20 mV.

Second, a real PEMFC was assembled using the Pt1–Ru/C as the anode, which underwent a continuous operation at 0.6 V under H_2-air testing condition for 40 h, **Figure R7a** (Figure S34a in the revised Supplementary Information). The polarization and power density plots of the PEMFC in both H_2-O_2 and H_2-air conditions were obtained before and after the continuous operation (**Figure R7b-c**, Figure S34b-c in the revised Supplementary Information). The results further confirm the exceptional stability of the Pt1-Ru/C anode catalyst.

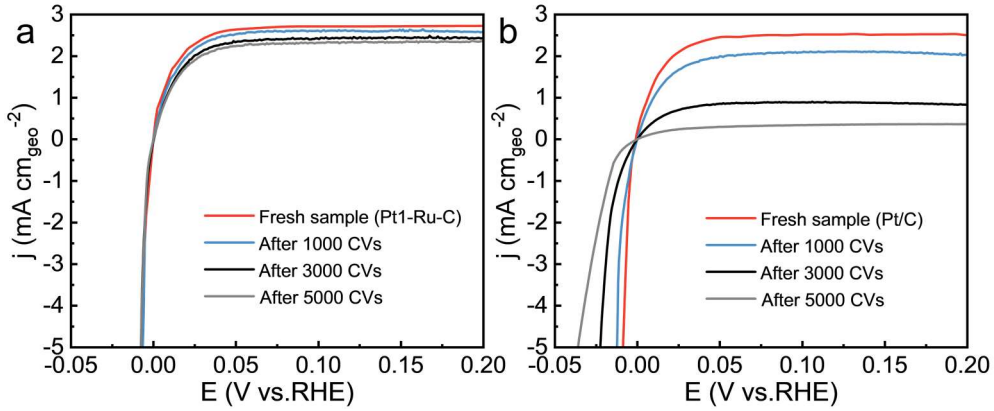

Figure R5. ADT results of a) Pt1-Ru/C and b) Ru/C in H_2-saturated 0.5 M H_2SO_4. The durability tests were performed by running repetitive CV scans from −0.05 to 0.1 V (vs. RHE) at a sweep rate of 150 mV s^{-1}. The LSV curves were recorded after 0, 1000, 3000, and 5000 CV scans, respectively.

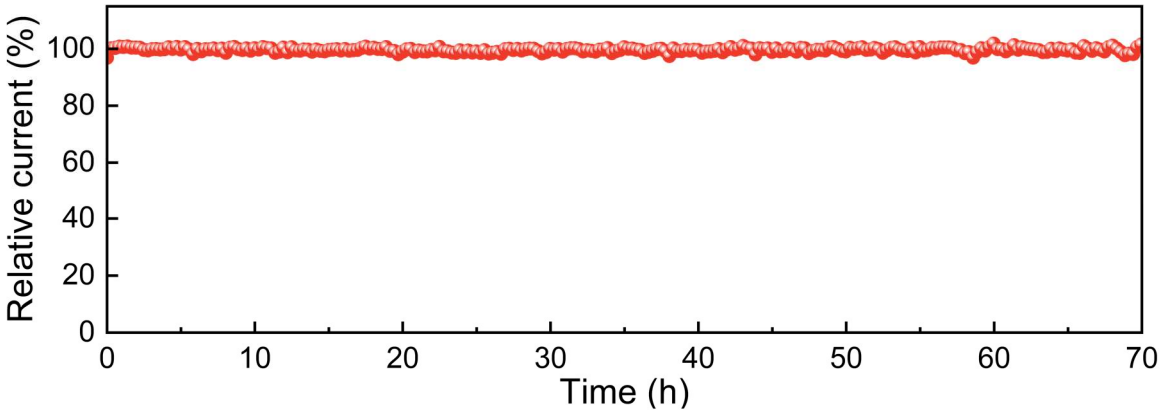

Figure R6. The HOR stability test. Relative current-time chronoamperometry response of Pt1-Ru/C in an H_2-saturated aqueous solution of 0.5 M H_2SO_4 at an overpotential of 20 mV.

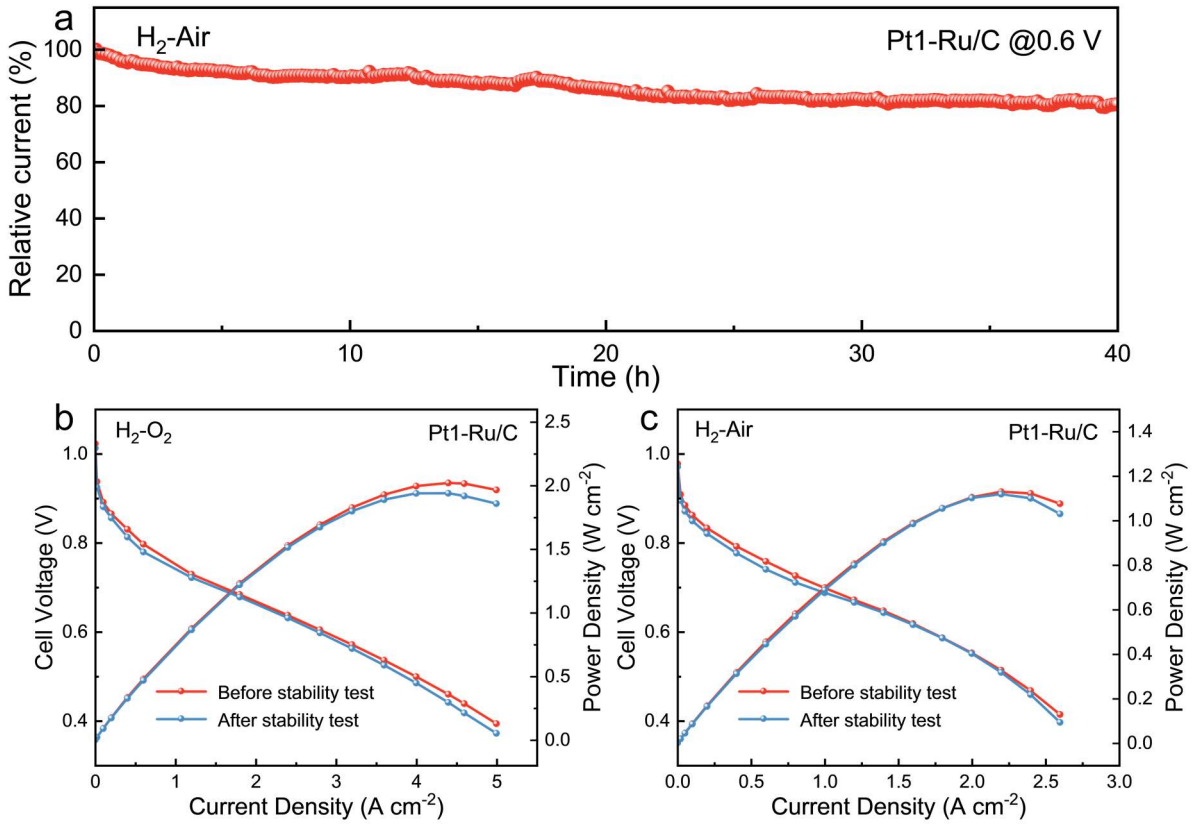

Figure R7. a) Long-term stability tests of the H_2-air PEMFC at 0.6 V using the Pt1-Ru/C (0.005 mg_{PGM} cm^{-2}) as the anode catalyst. Polarization and power density plots of the PEMFCs with the anode catalyst of Pt1-Ru/C before and after continuous operation at 0.6 V for 40 h under H_2-air condition. b) H_2-O_2 and c) H_2-air. Test conditions: cell temperature at 80 °C, H_2 flow rate at 1 L min^{-1} and O_2/Air flow rate at 2 L min^{-1}, symmetric back pressures at 250 kPa.

Comment 6: In Figure 4a, the change in the desorption peak potential is not clear. An arrow can be added to illustrate the trend of the peak potential change. According to Fig. 4d, what are the reasons for elevated limiting current densities?

Response to Comment 6: Thanks. Arrows have been added to illustrate the trend of the peak potential change in the updated Figure 4a and Figure S35 in the revised Supplementary Information (**Figure R8**).

As for the elevated limiting current densities in Figure 4g, we have re-measured the polarization curve and performed a kinetic isotope effect (KIE) analysis. As demonstrated in **Figure R9** (Figure 4g in the revised manuscript), the re-evaluated data shows uniform limiting current region.

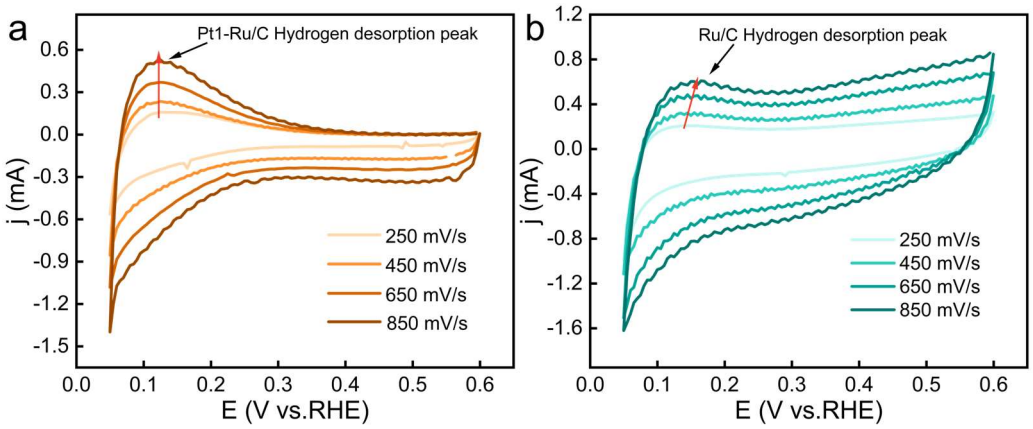

Figure R8. CV curves of Pt1-Ru/C (a) and Ru/C (b) catalyst with different scan rate in 0.5 M Ar-saturated H_2SO_4.

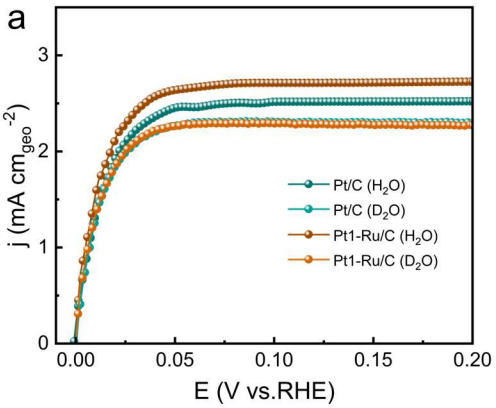

Figure R9. HOR polarization curves of Pt/C and Pt1-Ru/C catalysts in H_2-saturated 0.5 M H_2SO_4 aqueous solution and H_2-saturated 0.5 M D_2SO_4 deuterium oxide (D_2O) solution.

Comment 7: In Figure 5d, the names of the elements represented by different spheres should be marked.

Response to Comment 7: Thanks. The names of the elements corresponding to the spheres have been provided in the legend of Figure 5 in the revised manuscript.

Comment 8: Please elaborate on why the potential for comparing the KIE of the HOR is around 0.3-0.5 V. Explain why the 0.3-0.5 V range represents the mass transfer region. Is it possible to narrow or expand this mass transfer region?

Response to Comment 8: The H/D kinetic isotope effect (KIE) can reflect the H* transfer kinetics of chemical reactions. Generally, the KIE value exceeding 1.5 reveals that the reaction

involves H* transfer process (*Nat. Commun.* 2022, 13, 1189, *Nat. Commun.* 2019, 10, 5074). In the HOR process, H* are generated from the dissociation of H_2, and deuterium atoms in D_2O do not directly participate in the H_2 dissociation, H* adsorption, and H* desorption processes. Therefore, the kinetic current of HOR is not affected by the presence of D_2O (**Figure R10**, i.e. Figure S43 in the revised Supplementary Information).

However, compared with that in H_2O, the HOR diffusion-limiting current in D_2O is decreased due to the lower H_2 mass diffusion coefficient (Figure R9). Meanwhile, the mass transfer of H* also decreases in D_2O, which further decrease the diffusion-limiting current for the catalytic process with a hydrogen spillover behavior. Therefore, we compared the KIE in 0.3–0.5 V with the focus on diffusion-limiting region.

The region above 0.3 V is a sufficient but not necessary condition. In fact, the HOR current is controlled by H_2 mass transportation at potentials above 0.1 V, and the mass transfer region can be expanded to this value.

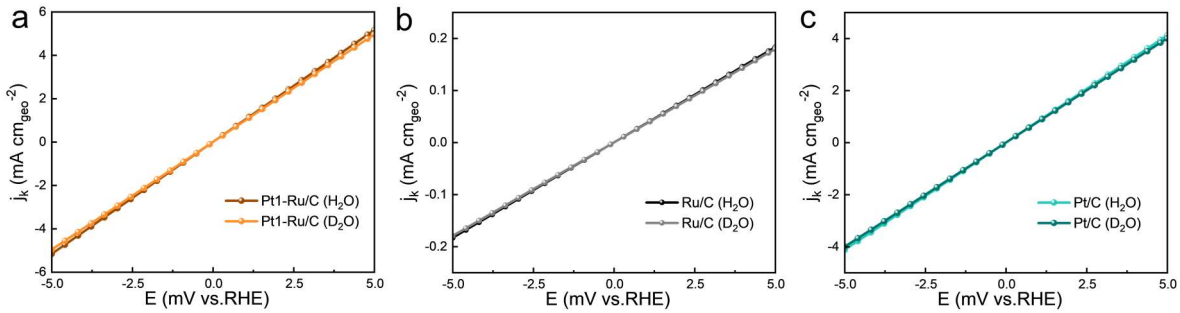

Figure R10. Linear region of kinetic current density (j_k) (calculated based on the Koutecky-Levich equation) of a) Pt1-Ru/C, b) Ru/C, and c) Pt/C.

Comment 9: According to Fig. S18, whether the Pt1/C catalyst does not have catalytic activity can be attributed to the unsuccessful loading of Pt on C.

Response to Comment 9: As demonstrated in the HAADF-STEM image in **Figure R11** (Figure S22a in the revised Supplementary Information), bright dots corresponding to Pt single atoms can be observed on the carbon support. The Pt content in Pt1/C is determined to be 0.102% based on ICP-MS (Table S1 in the revised Supplementary Information). Therefore, the low catalytic activity of Pt1/C should not be attributed to the unsuccessful loading of Pt.

The absence of HOR catalytic activity for Pt1/C may be attributed to the low Pt mass loading. As demonstrated in *Adv. Mater.* 2024, 36, 2404672 and *ACS Catal.* 2018, 8, 9, 8450–8458, Pt

single-atom catalysts may exhibit good HOR activity, where the loading of Pt single atoms exceeds 3 wt %.

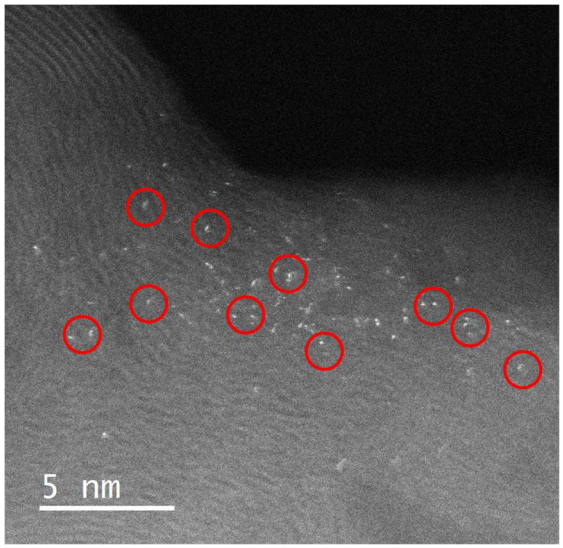

Figure R11. HAADF-STEM image and of Pt1/C.

Comment 10: Stability is a key indicator for evaluating the practical application potential of catalysts. Does Pt1-Ru/C have excellent catalytic stability and structural stability?

Response to Comment 10: The catalytic stability of Pt1-Ru/C has been provided in the response to comment 5.

As for the structural stability, we obtained the HAADF-STEM image of Pt1-Ru/C after the ADT. As depicted in **Figure R12** (Figure S27 in the revised Supplementary Information), HAADF-STEM images reveal no significant structural change on Pt1-Ru/C catalyst, suggesting excellent structural stability of Pt1-Ru/C. Relevant discussions have been updated on page 6 in the revised manuscript.

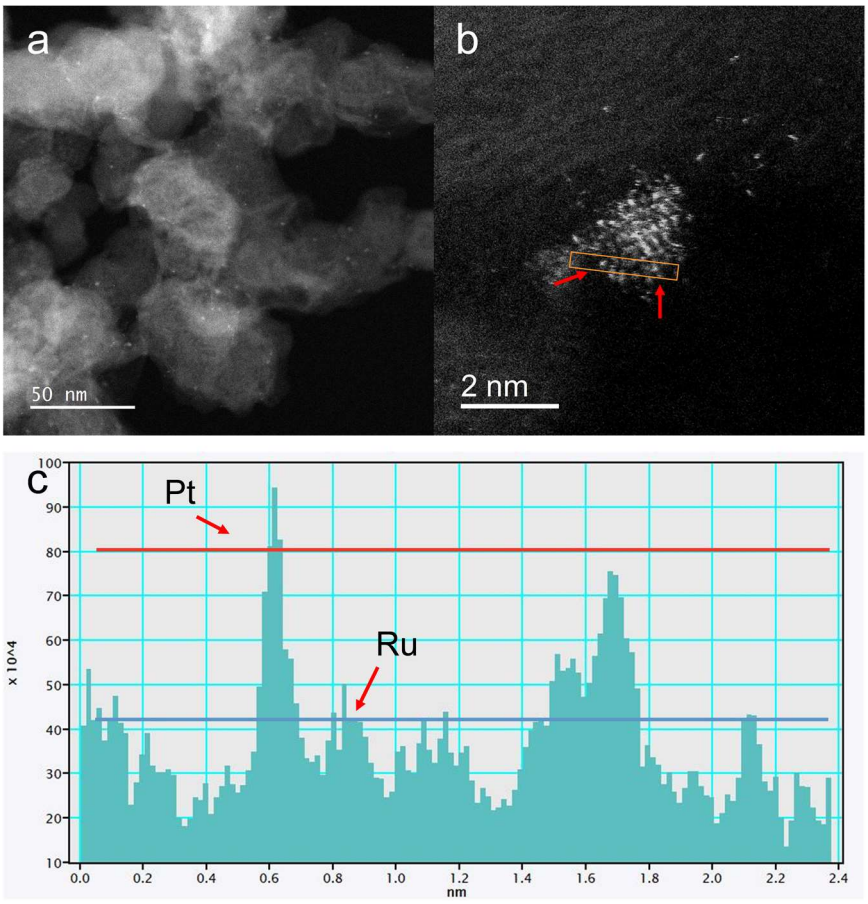

Figure R12. HAADF-STEM images and the intensity profiles (corresponding to the yellow boxed regions in Figure R12b) of Pt1-Ru/C after the accelerated durability test in 0.5 M H_2SO_4.

Comment 11: There are many grammar mistakes in this manuscript and the authors should check the manuscript.

Response to Comment 11: Thanks. We have double-checked the grammar and expressions throughout the manuscript and made necessary corrections.

Reviewer #2: The authors report an interesting Pt-Ru/C catalyst for the hydrogen oxidation reaction (HOR), attributing the enhanced performance to the hydrogen spillover effect from Ru to Pt. This catalyst achieves a peak power density of 1.91 W cm^{-2} at an ultralow loading of 5 μg_{PGM} cm^{-2}, meeting the DOE target. While the work presents promising results, I disagree with some of the explanations, and several aspects remain unclear or contain mistakes. Therefore, I believe a major revision is necessary.

Comment 1: It is unclear how the Pt-Ru catalyst is defined. Are Pt and Ru forming a composite or an alloy? Is Pt located on the surface of Ru clusters, or is there surface exchange between Pt and Ru to form an alloy structure? This distinction is crucial, especially for accurately constructing the model for DFT calculations. Based on the current characterization and analysis provided, the structure remains ambiguous. Please clarify with additional evidence or characterization.

Response to Comment 1: Based on the EXAFS results, Pt atoms do not form an alloy structure with Ru clusters. Typically, the Pt-Ru bonds in PtRu alloy structures locate at approximately 2.1 Å (*ACS Nano* 2009, 3, 10, 3127–3137, *J. Phys. Chem. C* 2008, 112, 50, 19922–19929, *Applied Catalysis A: General* 2007, 326, 194-201), as shown in **Figure R13**. In our case **(Figure R14)**, the Pt-Ru bond locates at around 2.65 Å, suggesting that Pt may locate on Ru cluster surface.

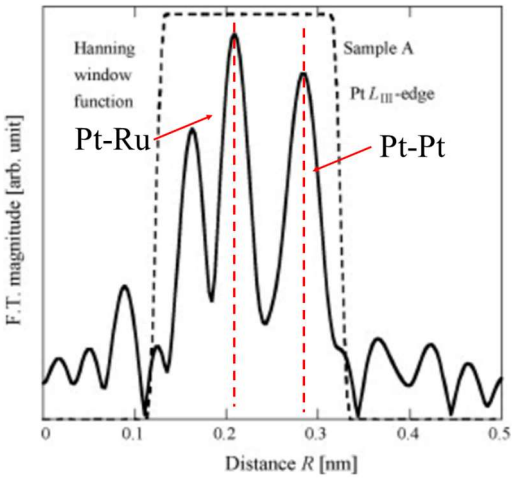

Figure. R13. Pt L_3-edge EXAFS spectra of PtRu alloy. Reproduced with permission (*Applied Catalysis A: General* 2007, 326, 194-201). Copyright © 2007 Published by Elsevier B.V.

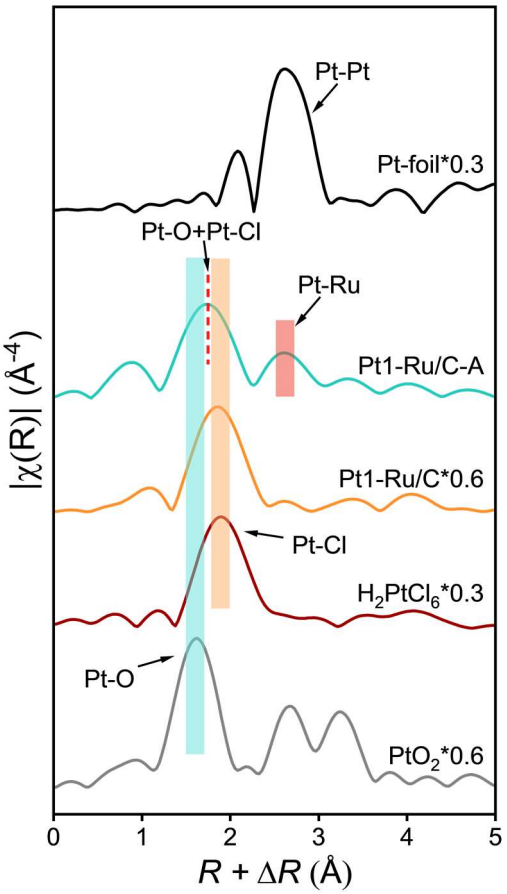

Figure R14. Pt L_3-edge EXAFS spectra of Pt-foil, Pt1-Ru/C-A, Pt1-Ru/C, H_2PtCl_6, and PtO_2.

Comment 2: While the catalyst demonstrates impressive peak power density, it is essential to present its stability performance. How does the catalyst perform over extended operation? Additionally, it would be valuable to compare your results with recent literature, focusing on peak power density, mass activity, and long-term stability.

Response to Comment 2: The durability of the PEMFC with the Pt1-Ru/C anode was evaluated through continuous operation at 0.6 V under H_2-air testing condition for 40 h (**Figure R15a**), and the polarization and power density plots of the PEMFC were obtained before and after the continuous operation in both H_2-O_2 and H_2-air conditions (**Figure R15 b-c**). The results further confirm the exceptional stability of the Pt1-Ru/C anode catalyst.

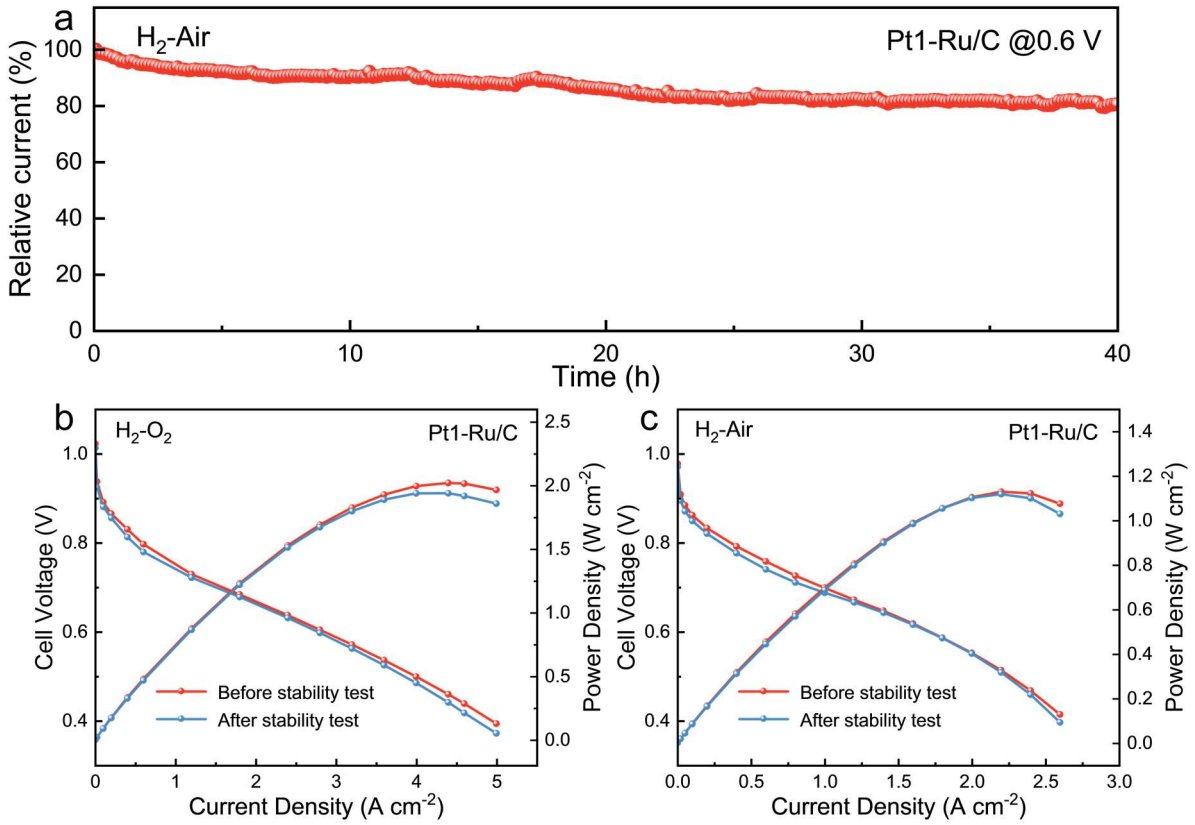

Figure R15. a) Long-term stability tests of the H_2-Air fuel cell at 0.6 V using the Pt1-Ru/C (0.005 mg_{PGM} cm^{-2}) as the anode catalyst. Polarization and power density plots of the PEMFC made with the anode catalyst of Pt1-Ru/C before and after the continuous operation at 0.6 V for 40 h under H_2-air condition. b) H_2-O_2 and c) H_2-air. Test conditions: cell temperature at 80 °C, H_2 flow rate at 1 L min^{-1} and O_2/air flow rate at 2 L min^{-1}, symmetric back pressures at 250 Kpa.

Moreover, we further compared the experimental data with recent literature reports on anode catalysts of the PEMFCs in terms of peak power density, mass activity, and long-term stability, as shown in **Figure R16** (Figure S31 in the revised Supplementary Information) and **Table R2** (Table S5 in the revised Supplementary Information). Specifically, the maximum power density (P_{max}) of cell with the Pt1-Ru/C anode catalyst reaches 1.91 W cm^{-2}, which is comparable to the state-of-the-art anode catalysts reported to date. The activity normalized by the anode PGM mass at 0.6 V is 520 A mg_{PGM}^{-1} under H_2-O_2 condition, which is surpass to other catalyst systems in reported PEMFCs. The results and the corresponding discussions have been updated on pages 7-8 in the revised manuscript.

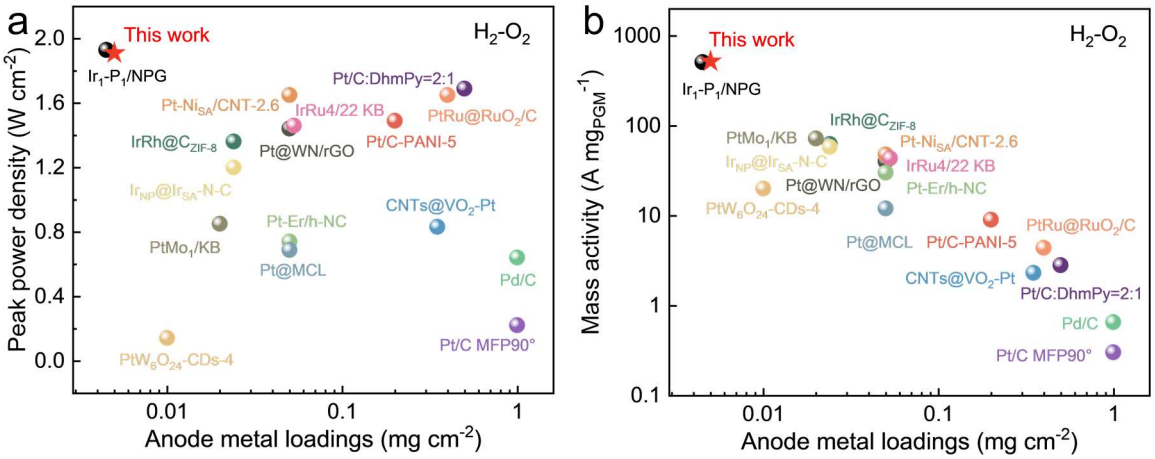

Figure R16. Comparisons of a) the peak power densities and b) the mass activity at 0.6 V normalized by the mass of anode metal of PEMFCs for H_2-O_2 as feeding gas (detail shown in Table S5).

Table R2. Performance comparison of the PEMFCs reported in literatures.

Anode (loading$_{PGM}$)	PPD (W/cm^2)	Anode mass activity @0.6 V (A mg$_{PGM}^{-1}$)	Stability	Ref.
Pt1-Ru/C (0.005 mg cm-$^{-2}$)	1.91 (O_2) 0.95 (Air)	520 260	20% current loss @0.6 V, 40 h (Air)	This work
Ir_1-P_1/NPG (0.0045 mg cm-$^{-2}$)	1.93 (O_2) 1.06 (Air)	511 333	30 mV voltage loss @1.0 A cm^{-2}, 35 h (O_2)	5
Pt@WN/rGO (0.05 mg cm^{-2})	1.442 (O_2) 0.826 (Air)	40 22	4.6% current loss @0.6 V, 50 h (O_2)	6
IrRh@C_{ZIF-8} (0.024 mg cm^{-2})	1.361 (O_2) -	62.5 -	-	7
Pd/C (1 mg cm^{-2})	0.64 (O_2) -	0.65 -	A constant current density @0.2 A cm^{-2}, 100 h (O_2)	8
$PtMo_1$/KB (0.02 mg cm^{-2})	0.85 (O_2) -	72.27 -	-	9

PtW_6O_{24}-CDs-4 (0.01 mg cm^{-2})	0.14 (O_2) -	20 -	0.8 V to 0.7 V @10 mA cm^{-2}, 12 h (O_2)	10
Ir_{NP}@Ir_{SA}-N-C (0.024 mg cm^{-2})	1.20 (O_2) -	58.01 -	-	11
Pt-Ni_{SA}/CNT-2.6 (0.05 mg cm^{-2})	1.65 (O_2) -	48 -	-	12
PtRu@RuO_2/C (0.4 mg cm^{-2})	1.65 (O_2) -	4.375 -	-	13
Pt/C-PANI-5 (0.2 mg cm^{-2})	1.49 (O_2) -	9 -	-	14
Pt/C:DhmPy=2:1 (0.5 mg cm^{-2})	1.69 (O_2) -	2.8 -	-	15
Pt/C MFP90° （1 mg cm^{-2}）	0.22 (O_2) -	0.3 -	-	16
PtSn/VC (3) (0.16 mg cm^{-2})	- 0.01 (Air)	- 0.8125	85% of PPD was retained after 60 000 cycles (Air)	17
Cu/Pt (0.5) (0.624 mg cm^{-2})	- 0.005 (Air)	- 0.096	A stable voltage @90 mA cm^{-2}, 5 h (Air)	18
IrRu4/22 KB (0.053 mg cm^{-2})	1.46 (O_2) -	43.4 -	-	19
Pt-Er/h-NC (0.05 mg cm^{-2})	0.74 (O_2) -	30 -	-	20
Pt@MCL (0.05mg cm^{-2})	0.687 (O_2) -	12 -	-	21
CNTs@VO_2−Pt (0.35 mg cm^{-2})	0.831 (O_2) -	2.3 -	A relatively constant voltage @0.9 V, 200 h (O_2)	22

Comment 3: Did the authors investigate the effect of varying Pt and Ru ratios in the catalyst? How do different weight percentages influence performance and hydrogen spillover? For instance, would increasing the Pt content improve the catalyst`s activity? Including such data would strengthen the conclusions.

Response to Comment 3: We controlled the loading of Pt single atoms anchored on Ru nanoclusters to investigate its impact on the catalytic performance and hydrogen spillover. The catalytic activity initially increases with the rising of the Pt single atoms density, as shown in **Figure R17 (**Figure S20a-b in the revised Supplementary Information). This phenomenon can be attributed to the fact that the hydrogen spillover effect between Pt-Ru is enhanced as the density of Pt single atoms increases. Once the saturation density of Pt single atoms on Ru nanoclusters is reached, additional Pt atoms cannot contribute the enhancement of HOR activity.

In addition, we supplement the H_2-TPD experiments to further confirm the effect of Pt loading on hydrogen spillover (**Figure R18**). The H_2 desorption peak temperature initially decreases and then stabilizes with increasing Pt loading, which further confirms that higher Pt loading enhances the hydrogen spillover effect before reaching the saturation coverage density. Beyond this saturation threshold, surplus Pt atoms demonstrate negligible capacity to facilitate spillover interactions with Ru clusters.

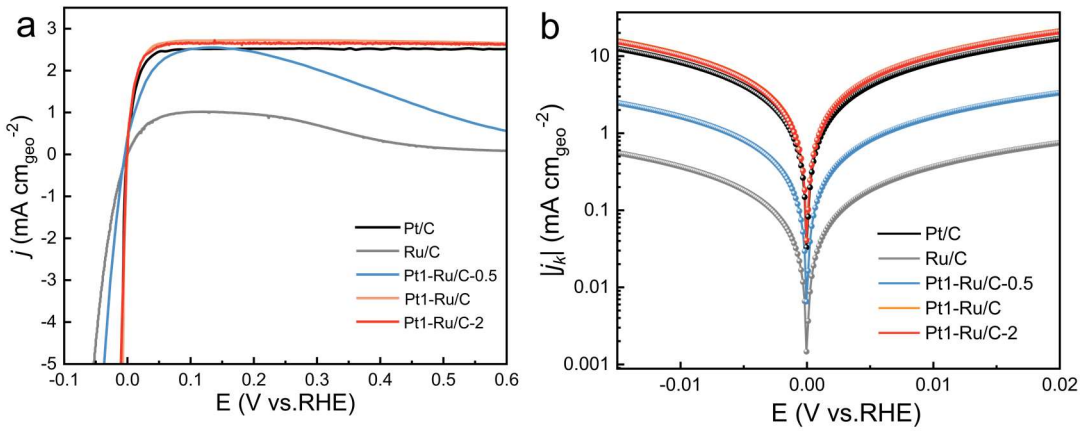

Figure R17. Electrochemical measurement results. a) Geometric area-normalized LSV curves of different catalysts. b) Calculated HOR kinetic current densities (j_k) versus potential plots recorded from (a).

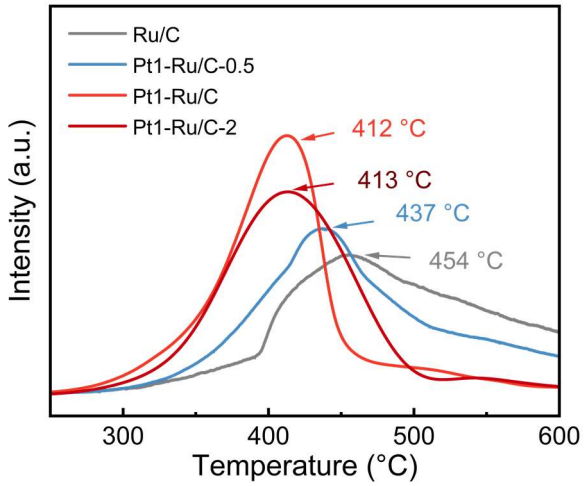

Figure R18. H_2-TPD profiles of Ru/C, Pt1-Ru/C-0.5, Pt1-Ru/C, and Pt1-Ru/C-2.

Comment 4: In Figure 3a-c, is there evidence of Ru dissolution during oxidation? If Ru dissolves, this could lead to Pt detachment. If this occurs, how is the sustained performance in Figure 3c explained? Please provide further discussion or experimental verification.

Response to Comment 4: To evaluate Ru dissolution behavior and its contribution to catalyst deactivation, the chronoamperometric measurement coupled with ICP-MS analysis were conducted at 0.4 V vs. RHE over a 120-minute duration, with sampling intervals at 1, 2, 5, 10, 20, 40, 60, 90, and 120 minutes. As shown in **Figure R19**, the dissolved Ru concentration in Pt1-Ru/C remains below the instrument detection limit (0.1 ppb) during the electrochemical testing, indicating that Ru does not undergo significant dissolution under an applied overpotential of 0.4 V.

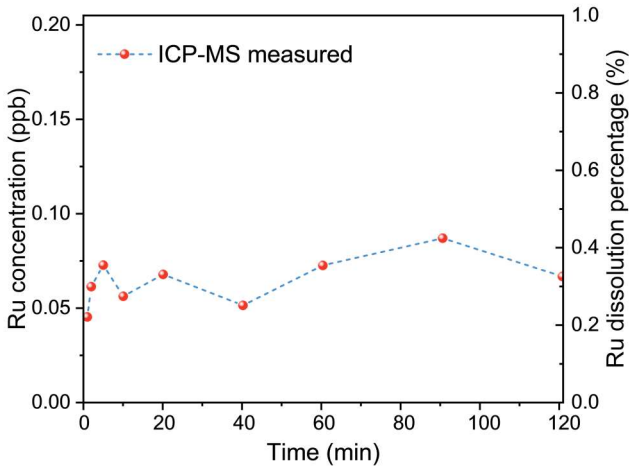

Figure R19. Ru concentration and dissolution percentage curves in electrolyte over time.

Comment 5: I agree that the KIE experiment supports the observation of faster kinetics for the HOR. However, I did not find a clear explanation of how this experiment specifically validates the proposed hydrogen spillover mechanism. Please elaborate on how the experimental results validate the spillover process or consider conducting additional experiments to substantiate this claim.

Response to Comment 5: Generally, a KIE value exceeding 1.5 reveals that the reaction involves H* transfer process (*Nat. Commun.* 2022, 13, 1189, *Nat. Commun.* 2019, 10, 5074). In the HER potential range, the KIE values for both Ru/C and Pt/C are below 1.5 (**Figure R20a** and Figure S42 in the revised Supplementary Information), while that for Pt1-Ru/C ranges from 2.2 to 3.6 (**Figure R20c**), which suggests that deuterium atoms participate in the hydrogen spillover process and decrease the HER rate accordingly.

During the HOR process, H* are generated from the dissociation of H_2, and deuterium atoms in D_2O are excluded from the hydrogen spillover process, leading to no significant effect of D_2O on the kinetic current of HOR (Figure S43 in the revised Supplementary Information). However, due to the lower H_2 mass diffusion coefficient in D_2O compared to that in H_2O (*Diffusion: mass transfer in fluid systems.* (Cambridge university press, 2009)), the limiting current of HOR decreases (**Figure R20b** and Figure S41 in the revised Supplementary Information). Furthermore, since the mass transfer rate of H* also decreases in D_2O, the catalysts that exhibit hydrogen spillover behavior will suffer from a more serious mass transfer

limitation in D_2O and hence a higher KIE value. In the limiting current potential range (0.1 V to 0.5 V vs. RHE), the KIE value for Pt1-Ru/C (1.2) is slightly higher than Pt/C (1.1), and Ru/C (1.1) (**Figure R20c** and Figure S44 in the revised Supplementary Information). Therefore, these results evidence the hydrogen spillover process for Pt1-Ru/C.

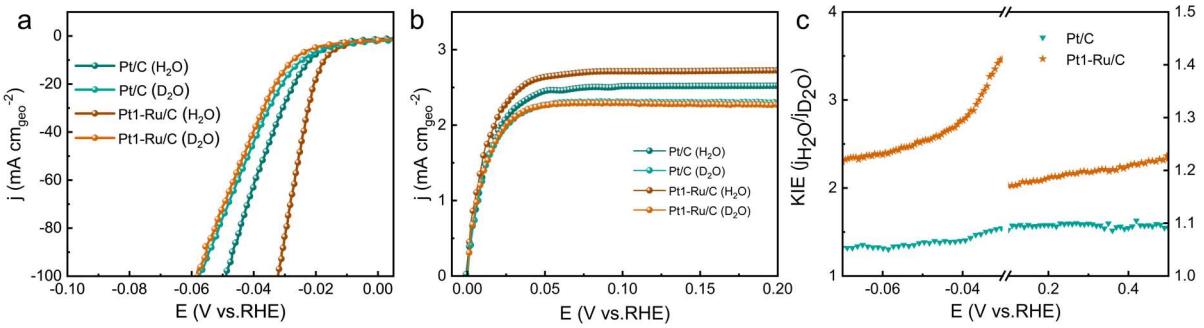

Figure R20. a) HER polarization curves of Pt/C and Pt1-Ru/C catalysts in N_2-saturated 0.5 M H_2SO_4 aqueous solution and N_2-saturated 0.5 M D_2SO_4 deuterium oxide (D_2O) solution. b) HOR polarization curves of Pt/C and Pt1-Ru/C catalysts in H_2-saturated 0.5 M H_2SO_4 aqueous solution and H_2-saturated 0.5 M D_2SO_4 deuterium oxide (D_2O) solution. c) H/D isotope effect analysis (j_{H_2O}/j_{D_2O} *vs.* potential) for Pt/C and Pt1-Ru/C.

Comment 6: Figure 2 is missing sub-labels (a, b, c, d). Please revise to ensure clarity and consistency.

Response to Comment 6: Thanks. We have added sub-labels to Figure 2 in the revised manuscript.

Comment 7: In the supporting information, the notation in catalyst names, such as "Pt1-Ru/C-0.5-A" and "Pt1-Ru/C-2-A," is unclear. What do the numbers "1," "-0.5," and "-2" represent? Providing a clear explanation of this naming convention would help readers better understand the catalyst variations.

Response to Comment 7: Thanks. We have added an explanation for the nomenclature. Relevant discussions have been provided on page 1 in the revised Supplementary Information, as follows:

For Pt1-Ru/C-x catalysts, Pt1 represents single-atom Pt, Ru denotes Ru nanoclusters, C stands

for the carbon support, and x indicates the amount of H_2PtCl_6 (with 60 μL as the baseline volume) used during impregnation.

For example: Pt1-Ru/C refers to the catalyst prepared by impregnating 20 mg of Ru/C with 60 μL of 0.01 M H_2PtCl_6 solution (x=1, which is omitted for simplicity). Pt1-Ru/C-2 corresponds to the catalyst prepared by impregnating 20 mg of Ru/C with 120 μL of 0.01 M H_2PtCl_6 solution (i.e., x=2).

Additionally, Pt1-Ru/C-x-A represents the Pt1-Ru/C-x catalyst after activation under HOR overpotentials.

Comment 8: The manuscript lacks details on the EXAFS fitting procedure. Please describe the fitting process in detail, including fitting parameters, reference models, and error analysis.

Response to Comment 8: We have supplemented the EXAFS fitting details. Relevant discussions have been provided on pages 18-19 in the revised manuscript and page 53 in the revised Supplementary Information, as follows:

The normalized EXAFS spectra were obtained by subtracting the post-edge background from the overall absorption and then normalizing the edge-jump step. For the EXAFS part, the Fourier-transformed data were fitted in R space. The passive electron factors, S_0^2, were determined by fitting the experimental Pt-foil and Ru-foil data, and then fixed for further analysis of the measured samples. The parameters described by the local structure environment including coordination numbers (N), bond distance (R), and Debye-Waller (σ^2) factor around the absorbed atoms were allowed to vary during the fit process. The quantitative structural parameters were obtained by a least-squares curve parameter fitting for the EXAFS spectra by ARTEMIS module. The continuous Cauchy wavelet transform (CCWT) methodology deconvolved the data. The Cauchy wavelet was chosen as the basis mother wavelet and the Cauchy order was set as 200 for a better analysis.

S_0^2 were set to 0.831 and 0.923 for Pt and Ru, respectively, according to the experimental EXAFS fit of Pt-foil and Ru-foil by fixing N as the known crystallographic value.

N - coordination numbers;

R - bond distance (the bond length between central atoms and surrounding coordination atoms);

σ^2 - Debye-Waller factors (a measure of thermal and static disorder in absorber-scatterer

distances);

ΔE_0 - the inner potential correction;

R factor – the goodness of fit.

Error bounds that characterize the structural parameters obtained by EXAFS spectroscopy were estimated as N ± 20%; R ± 1%; σ 2 ± 20%; ΔE_0 ± 20%. For comparison, the interatomic distances and coordination numbers for the references (Ru-foil, H_2PtCl_6, and PtO_2) were calculated from their crystallographic structures.

Reviewer #3: This work, using Pt1-Ru/C catalyst as a model catalyst, demonstrates a tandem electrocatalysis to decouple the HOR process, and shows a high-performance Ru-based tandem HOR electrocatalyst for PEMFCs. The reaction mechanism is studies through both experimental and theoretical methods. The following concerns are still need to be addressed.

Comment 1: In Figures 1b and S6d, high-contrast bright spots are distinctly distributed not only on the Pt1Ru nanoparticles but also on the carbon support. These metallic sites on the support may also exhibit catalytic activity during reactions. The authors should further elucidate the catalyst structure and investigate whether synergistic effects exist between Pt/Ru single atoms on the support and the Pt1Ru nanoparticles.

Response to Comment 1: Overall, the Pt/Ru single-atom remaining on the carbon support exhibit negligible HOR activity and show no detectable synergistic effects with Pt1Ru nanoparticles.

First, the bright spots observed in the HAADF-STEM images (Figures 1b and S6d) correspond to dispersed Pt atoms on the carbon support. To probe the catalytic contribution of metallic Pt single atoms on the support, we synthesized a model catalyst comprising isolated Pt single-atom catalysts anchored on the carbon (denoted as Pt1/C). As shown in **Figure R21** (Figure S21 in the revised Supplementary Information), the Pt1/C sample exhibits negligible HOR activity. Further, we modulated the Pt single-atom loading on the catalyst. If synergistic interactions existed between Pt single atoms on the carbon and Ru/Pt1-Ru nanoclusters, the HOR activity would exhibit a monotonic improvement with increasing Pt single-atom density. However, once the saturation density of Pt single atoms on Ru nanoclusters is reached, further increasing the Pt single-atom density on the carbon support failed to enhance HOR performance (**Figure R22**). This phenomenon disproves the existence of synergistic effects between Pt single atoms and Ru/Pt1-Ru nanoclusters.

Second, the few Ru single atoms are possibly anchored on the carbon support as indicated by the relatively low-contrast bright spots in STEM images compared with Pt single atoms (Figure 1b). This is probably due to the anchoring effect of defect sites on the support, which stabilizes the isolated Ru species during the formation of Ru nanoclusters. These isolated Ru sites are also present in the Ru/C catalyst. Their negligible contribution to HOR activity is demonstrated

by the poor performance of Ru/C (Figure 2a in the revised manuscript), implying that the absent of synergistic effects between Ru single atoms on the support and the nanoparticles.

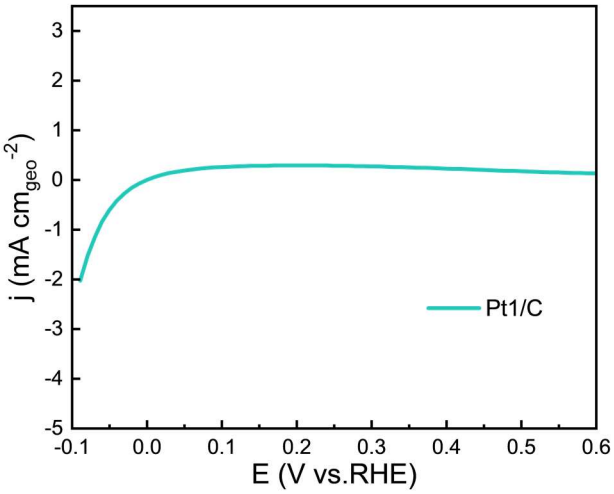

Figure R21. Geometric area-normalized LSV curves of Pt1/C.

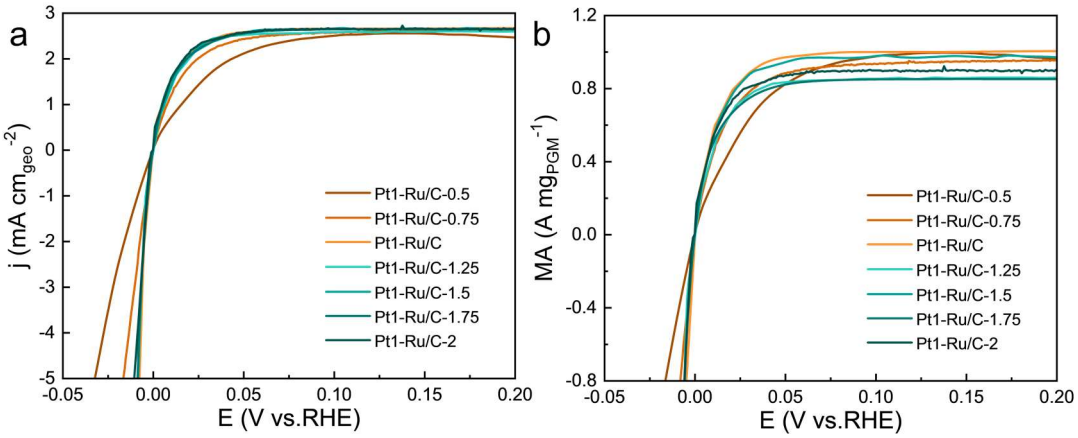

Figure R22. (a) HOR and (b) mass-normalized HOR polarization curves of different catalysts in H_2-saturated 0.5 M H_2SO_4 with a scanning rate of 5 mV s^{-1} at 1,600 rpm.

Comment 2: On Page 4, Lines 101 – 102, "Pt exists in the form of Cl-coordinated single atom in Pt1-Ru/C (Figure 1d-e and Figure S11), …" was mentioned. Following on from the previous question, the coordination of Cl may only be on the Pt1/C sites, while the coordination of Pt on the Pt1Ru nanoparticles may be different.

Response to Comment 2: We conducted a more detailed analysis of the coordination structure of Pt1-Ru/C using continuous Cauchy wavelet transform (CCWT) analysis, which reveals no

significant differences between the coordination environments of Pt atoms anchored on the carbon support and those within Ru clusters. Relevant discussions have been provided on pages 4-5 in the revised manuscript.

As shown in **Figure R23**, no additional coordination environments beyond Pt-Cl bonding were detected in the Pt1-Ru/C system. The only observable structural difference between Pt sites in Ru nanoclusters and isolated Pt single atoms on the carbon support manifests as a reduced Pt-Cl coordination number in Pt1-Ru/C relative to Pt1/C, as quantified by EXAFS fitting (Table S3 in the revised Supplementary Information). The observation indicates that the presence of Ru nanoclusters slightly attenuates the Pt-Cl anchoring strength without generating new coordination configurations. This phenomenon possibly arises from the electron transfer from Ru nanoclusters to $PtCl_6^{2-}$ precursors, which induces further reduction of the Pt sites and reduces of Pt-Cl coordinate numbers.

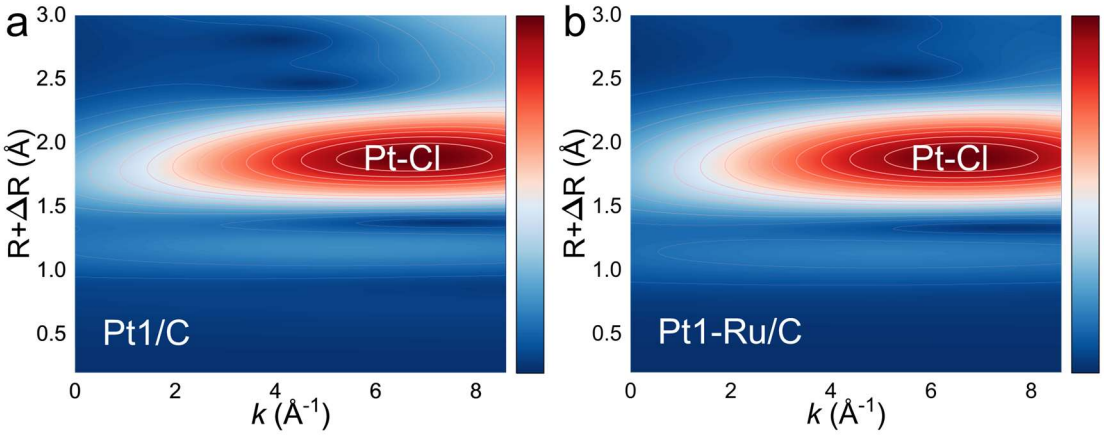

Figure R23. The corresponding continuous Cauchy wavelet transform (CCWT) for the k^3-weighted EXAFS signals at the Pt1/C (a) and Pt1-Ru/C (b).

Comment 3: For the XAS analysis, typical M-M coordination, i.e. Pt-Ru, should also exist in the Pt1Ru particles but missing in the provided data analysis. Please explain or recheck it.

Response to Comment 3: We further analyzed the EXAFS results of different samples by employing continuous Cauchy wavelet transform (CCWT) analysis, revealing distinct Pt-Ru coordination in the Pt1-Ru/C-A samples. Relevant discussions have been provided on pages 4-5 in the revised manuscript.

As depicted in **Figure R24a**, a distinct metal coordination at 2.65 Å emerges in the Pt1-Ru/C-A. The Pt1-Ru/C-A sample displays the k-space position of the metal-metal coordination centered at 7.0 $Å^{-1}$, lower than the Pt-Pt bond in Pt-foil (9.8 $Å^{-1}$) (**Figure R24b**). The downshift of the central position in k-space indicates the presence of lighter elements in the coordination shell, i.e. Pt-Ru in our case. The phenomenon may be attributed to the activation process triggering structural reconstruction of Pt1-Ru nanoclusters. Based on the above findings, we re-fit the EXAFS spectra of the Pt1-Ru/C-A. The coordination number for the Pt-Ru bonds are determined to be 0.7, as detailed in Figure S10 and Table S3 (in the revised Supplementary Information).

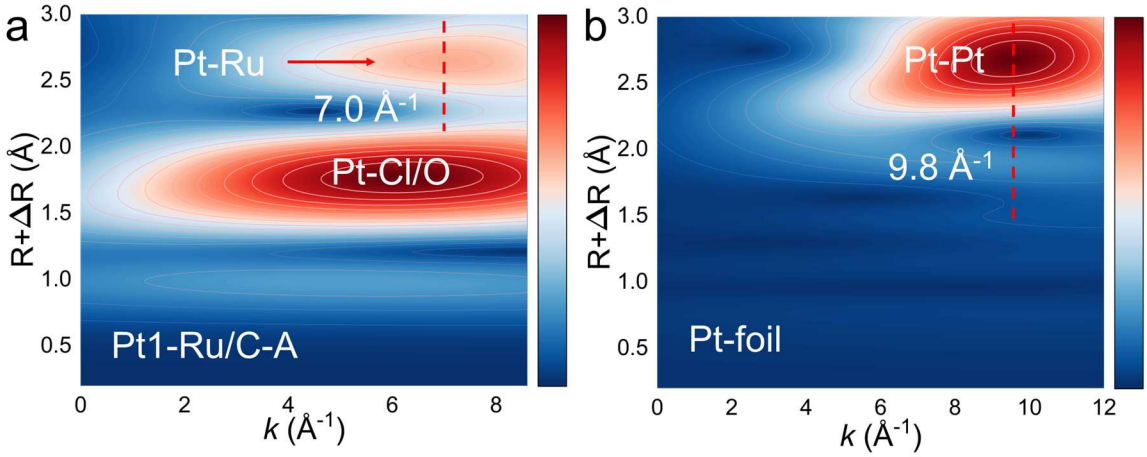

Figure R24. The corresponding Cauchy Wavelet Transform (CCWT) for the k^3-weighted EXAFS signals at the Pt1-Ru/C-A (a) and Pt-foil (b).

Comment 4: The statement in lines 110-111 claims "Pt is further reduced and converted into oxygen-coordinated single atoms during the HOR process". However, there is a causal link between this structural evolution and the enhanced HOR performance. To strengthen the mechanistic rigor, please discuss the structure-activity relationship between Pt-O coordination and HOR.

Response to Comment 4: In H_2-containing reducing environments, the Pt-Cl coordination exhibits thermodynamic instability (*Adv. Colloid Interface Sci.* 2020, 286, 102300). Following the cleavage of the Pt-Cl bond, the inherently high surface energy of Pt single atoms drives spontaneous adsorption of oxygen-containing species, ultimately stabilizing as Pt-O-coordinated single-atom structures (*Nat Commun*. 2022, 13, 6875). The formation of Pt-O

coordination is thermodynamically favored for stabilizing Pt single atoms under operational conditions. In other words, all Pt species discussed in this work inherently adopt oxygen-coordinated configurations, and the mechanistic analysis is based on this default premise.

Additionally, as confirmed by the updated DFT mechanistic diagrams in **Figure R25** (Figure 6 in the revised manuscript), the Pt-O coordinated single atoms demonstrate pronounced hydrogen spillover effects with adjacent Ru nanoclusters. Specifically, the free energy for direct desorption of H* from Ru and Pt sites are 0.44 and 0.31 eV, respectively (Figures S45-46 in the revised Supplementary Information). In contrast, the free energy for hydrogen spillover from Ru to Pt single atoms and desorption from Pt single atoms are 0.16 eV and 0.23 eV, respectively (**Figure R25a-b**). The decoupled HOR enabled by the hydrogen spillover effect not only reduces the desorption free energy of H* at Ru sites but also lowers the energy barrier of the rate-determining Volmer step.

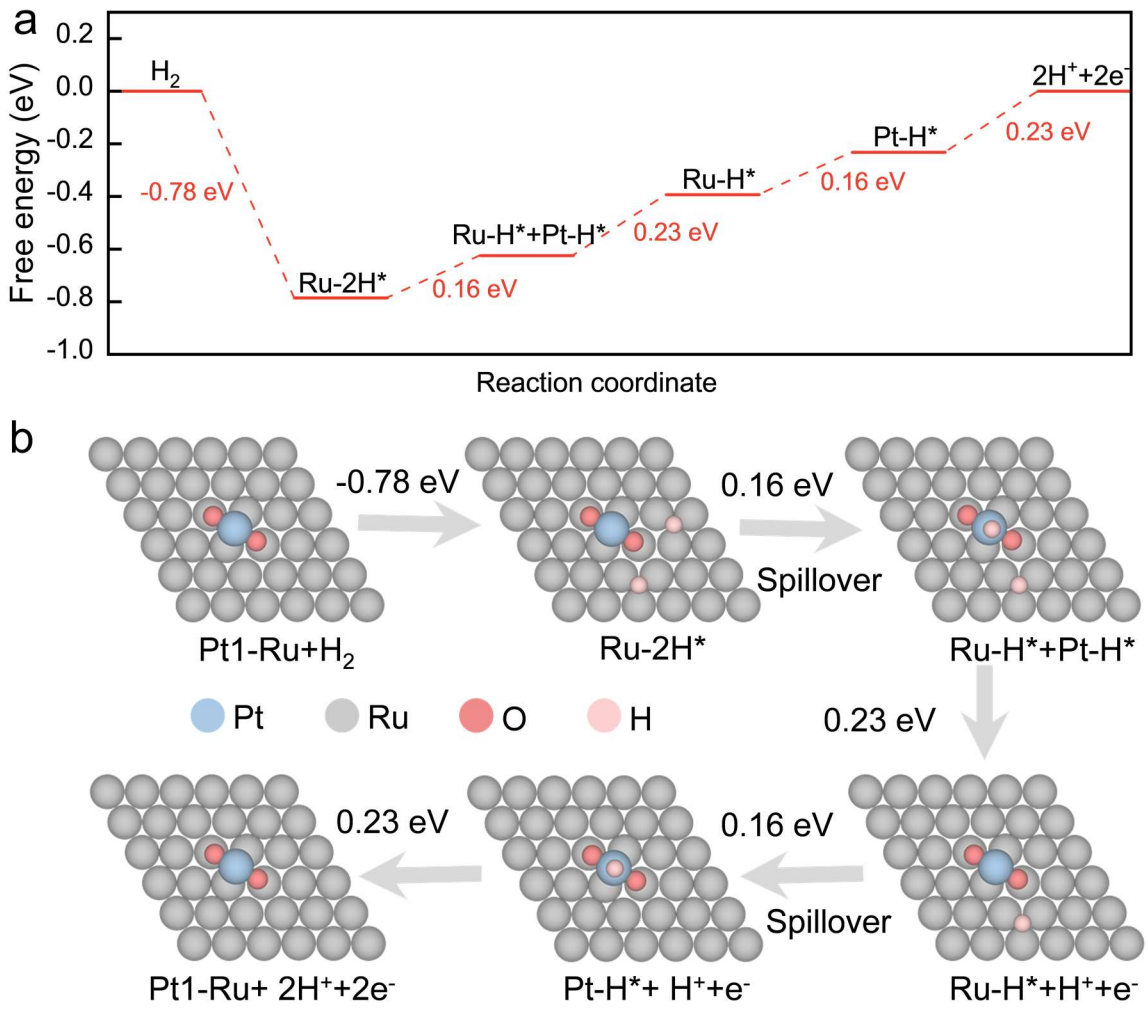

Figure R25. Theoretical calculation investigations. a) Gibbs free energy diagram for HOR on Pt1-Ru. b) Pt1-Ru models and schematic diagrams of the hydrogen spillover process as well as the corresponding free energy of each step.

Comment 5: The use of mass-normalized current density at 50 mV overpotential (Figure S17d) to evaluate and compare the mass activity of catalysts in this study appears insufficiently rigorous and accurate. As evident from Figure 2a, the current density of both Pt1-Ru/C and Pt/C at 50 mV overpotential have approached (or even reached) the limiting diffusion current density (jl). This strongly suggests that the reported current density at 50 mV is dominated by H_2 mass transport rather than intrinsic kinetics, rendering it unsuitable for evaluating true mass activity. In HOR research, the universally accepted standard metrics for mass activity are the following: (1) Mass-normalized exchange current density (j0,m) derived from kinetic analysis (e.g., Tafel fitting in the low-overpotential region); (2) Mass-normalized kinetic current density (jk,m) corrected for mass transport limitations at a defined overpotential interval (10~50 mV), typically via rotating disk electrode (RDE) measurements. I suggest recalculating the mass activity using $j_{0,m}$ and $j_{k,m}$ to enable a rigorous comparison.

Response to Comment 5: Thanks. we have updated the comparison of HOR performance in **Figure R26** (Figure S20 in the revised Supplementary Information), including kinetic current density (j_k), mass-normalized kinetic current density ($j_{k,m}$), current density (j) at an overpotential of 20 mV, exchange current density (j_0), and mass-normalized exchange current density ($j_{0,m}$). Relevant discussions have been provided on page 20 in the revised Supplementary Information.

As manifested in **Figure R26d**, the Pt1-Ru/C catalyst possesses the $j_{0,m}$ of 10.41 A mg_{PGM}^{-1}, which is higher than those of Pt/C (1.73 A mg_{PGM}^{-1}), Ru/C (0.43 A mg_{PGM}^{-1}), Pt1-Ru/C-0.5 (1.71 A mg_{PGM}^{-1}), and Pt1-Ru/C-2 (8.82 A mg_{PGM}^{-1}). At an overpotential of 20 mV, the Pt1-Ru/C catalyst demonstrates a mass-normalized kinetic current density ($j_{k,m}$) of 8.3 A mg_{PGM}^{-1}, surpassing Pt/C (1.4 mg_{PGM}^{-1}) by fivefold.

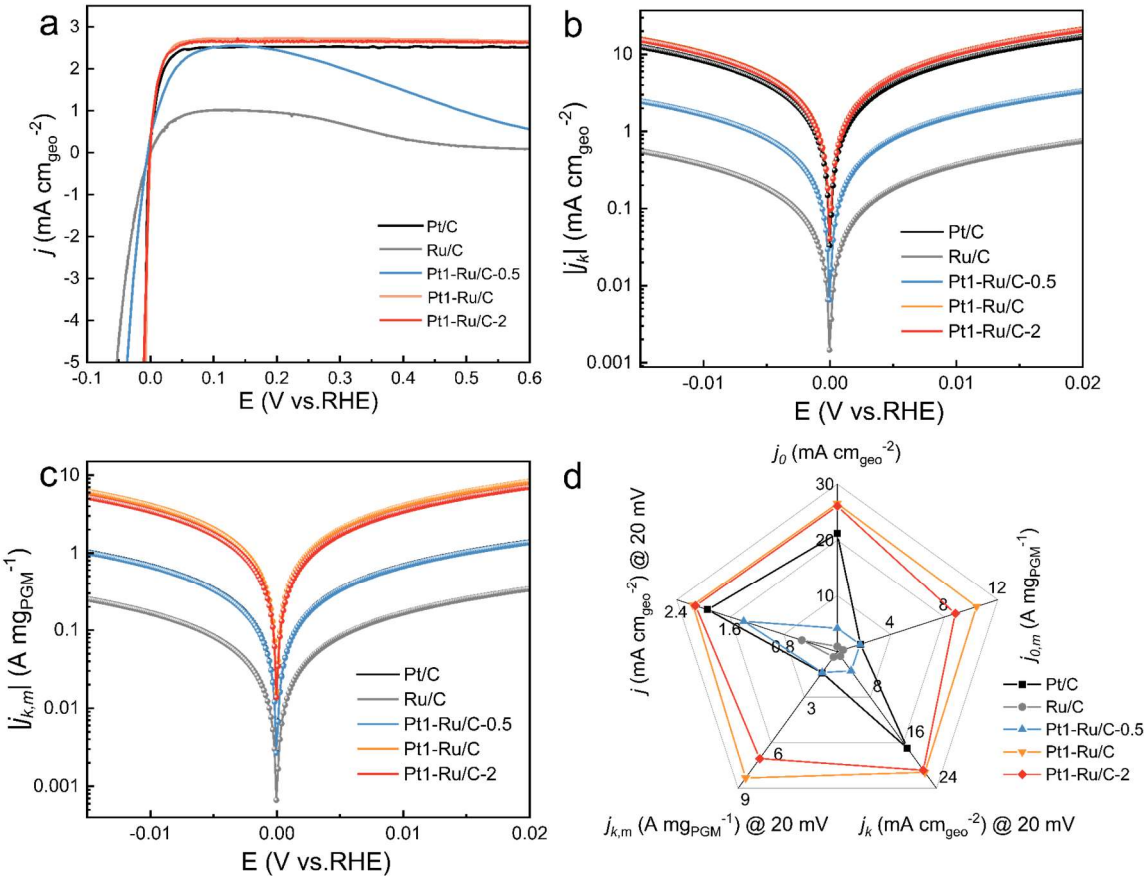

Figure R26. Electrochemical measurement results. a) Geometric area-normalized LSV curves of different catalysts. b) Calculated HOR kinetic current densities (j_k) versus potential plots recorded from (a). c) PGM mass-normalized HOR kinetic current densities (j_k) versus potential plots. d) Comparison of j_k, $j_{k,m}$ (mass-normalized j_k), and j at an overpotential of 20 mV and j_0, $j_{0,m}$ (mass-normalized j_0) of different catalysts.

Comment 6: Regarding the hydrogen spillover mechanism, the authors should supplement more experiments (such as in-situ impedance tests) to provide evidence. The difference in *H adsorption energy between Ru and Pt from theoretical calculations is insufficient to fully demonstrate the occurrence of hydrogen spillover.

Response to Comment 6: Thanks. We have supplemented the *in situ* electrochemical impedance spectroscopy (EIS) investigations to demonstrate the occurrence of hydrogen spillover. Relevant discussions have been provided on page 11 in the revised manuscript.

As shown in **Figures R27-28** (Figures S37-38 in the revised Supplementary Information) and Table S7 in the revised Supplementary Information, the recorded Nyquist plots were simulated by a double-parallel equivalent circuit model. The second parallel component R_2 (R_2 represents

the hydrogen adsorption resistance) can reflect the hydrogen adsorption behavior on catalyst surface. The hydrogen adsorption kinetics of different catalysts are quantified by plotting logR_2 vs. overpotential and calculating the EIS-derived Tafel slopes. As shown in **Figure R29** (Figure S39 in the revised Supplementary Information), the smaller EIS-derived Tafel slope for Pt1-Ru/C indicates an accelerated hydrogen adsorption kinetics. Such a phenomenon revealed that the existence of hydrogen spillover process.

Second, the evidence of hydrogen spillover in this research extends beyond the theoretical calculations. In the manuscript, we have provided a series of experimental evidences including scan-rate dependent H* desorption peak analysis (Figure 4a-b in the revised manuscript), HER Tafel slope characterization (Figure 4c-d in the revised manuscript), pH-dependent HER activity measurements (Figure 4e in the revised manuscript), isotope effect studies (Figure 4f-h in the revised manuscript), H_2 temperature-programmed desorption (H_2-TPD) (Figure 4i in the revised manuscript), and *in situ* synchrotron-based ATR-FTIR spectroscopy (Figure 5a-c in the revised manuscript). These experimental approaches collectively provide conclusive evidence for the occurrence of hydrogen spillover effects.

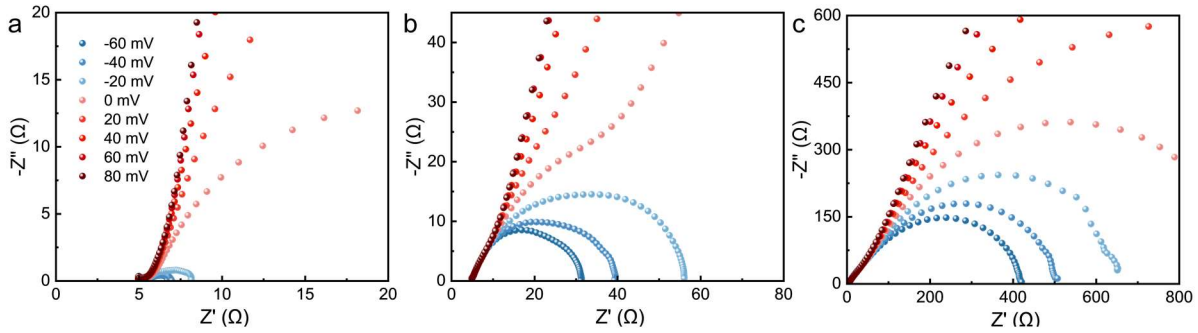

Figure S27. *In-situ* EIS plots on a) Pt1-Ru/C, b) Pt/C, c) Ru/C. The EIS was measured at different overpotentials in H_2-saturated 0.5 M H_2SO_4 solution with an amplitude voltage of 5 mV in a frequency range of 100 kHz-0.1 KHz.

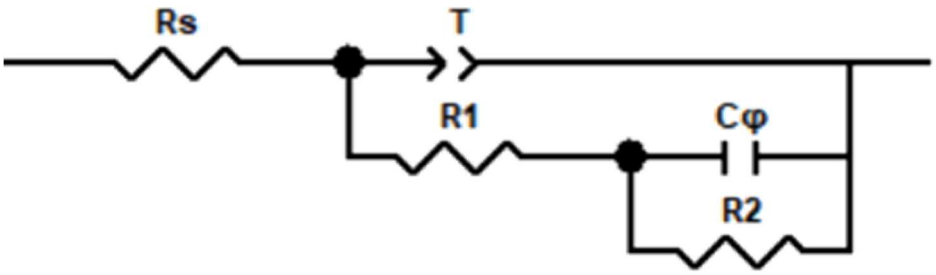

Figure S28. The equivalent circuit for the EIS simulation. Rs represents the solution resistance. T and R_1 represent the double layer capacitance and the catalytic charge transfer resistance, respectively. C_φ and R_2 are the hydrogen diffusion and adsorption pseudo-capacitance and resistance, respectively.

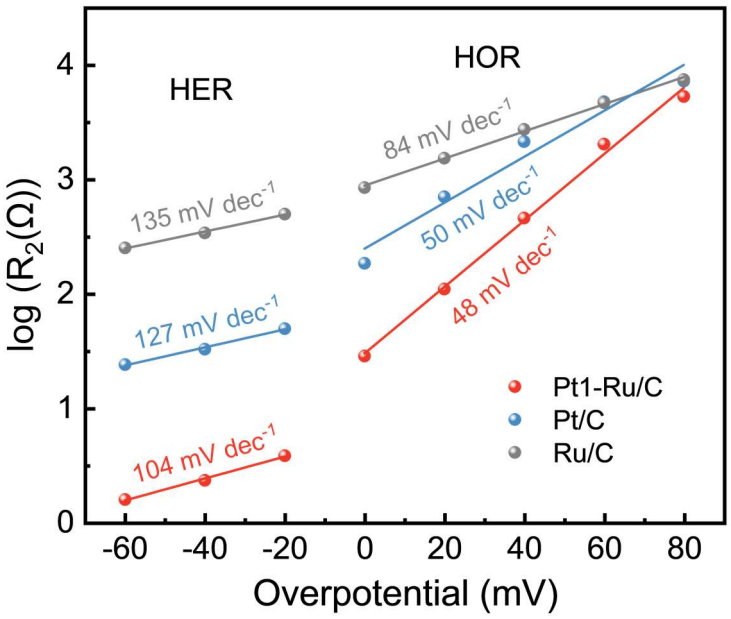

Figure S29. EIS-derived Tafel plots of the different catalysts.

Comment 7: For PEMFCs, the CO poisoning resistance of anode hydrogen oxidation reaction (HOR) catalysts is a critical metric for practical device applications. The authors should supplement the study with experiments (e.g., CO stripping voltammetry or tolerance tests under CO-containing atmospheres) to demonstrate the anti-CO poisoning performance of the catalysts.

Response to Comment 7: We have provided CO stripping voltammetry and tolerance tests under CO-containing atmospheres in the revised Supplementary Information. Relevant discussions have been provided on page 7 in the revised manuscript.

As depicted in **Figure R30** (Figure S29 in the revised Supplementary Information), the Pt1-Ru/C catalyst demonstrates outstanding resistance to CO poisoning, as evidenced by the chronoamperometry test at 0.1 V (vs. RHE) in H_2/1000 ppm CO-saturated 0.5 M H_2SO_4 solution, which might be attributed to the weakened CO adsorption capability of Ru induced

by electron transfer from Ru to Pt. Additionally, the CO-stripping experiments in a CO saturated electrolytes were conducted to assess the CO resistance of Pt1-Ru/C. As illustrated in **Figure R31** (Figure S30 in the revised Supplementary Information), the Pt1-Ru/C catalyst exhibits a significantly lower onset potential for CO stripping compared with Ru/C and Pt/C catalysts, which is consistent with its superior CO tolerance.

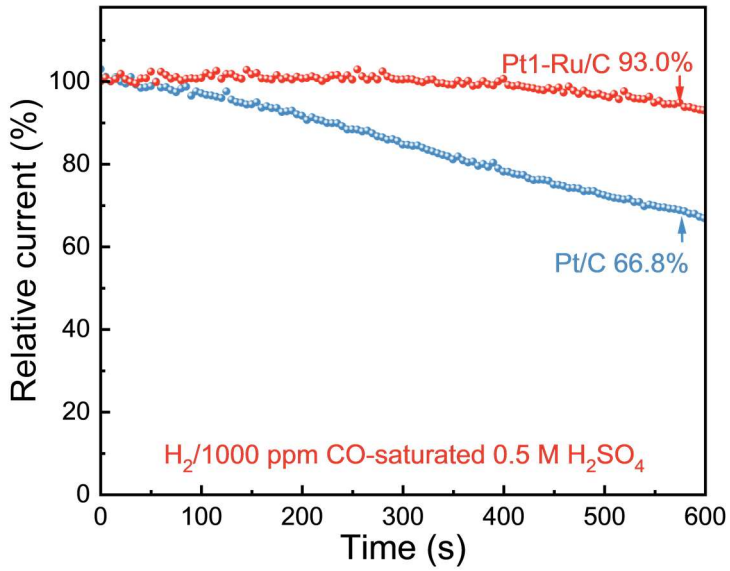

Figure R30. Relative chronoamperometry response of Pt1-Ru/C and Pt/C in H_2/1000 ppm CO-saturated 0.5 M H_2SO_4 solution at 0.1 V (vs. RHE).

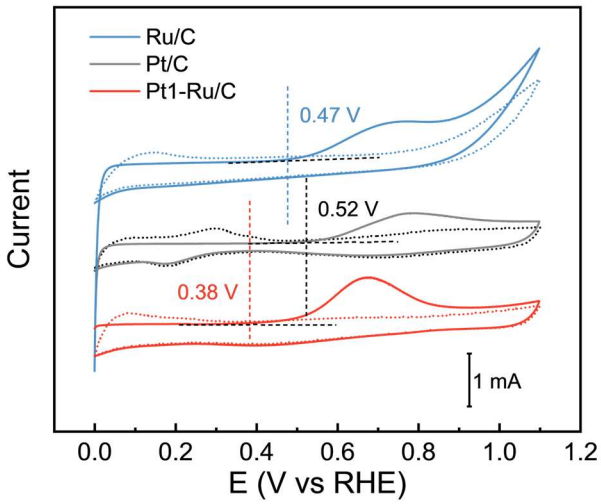

Figure R31. CO-stripping measurements for Pt1-Ru/C, Ru/C, and Pt/C.

Comment 8: For PEMFCs test, the absence of long-term durability significantly limits its practical relevance. For catalyst benchmarking in fuel cells, stability under realistic operating conditions is a critical metric for industrial applicability. I suggest the authors to conduct stability measures.

Response to Comment 8: Thanks. The durability of the PEMFC with the Pt1-Ru/C anode was evaluated through continuous operation at 0.6 V under H_2-air testing condition for 40 h (**Figure R32a**), and the polarization and power density plots of the PEMFC were obtained before and after the continuous operation in both H_2-O_2 and H_2-air conditions (**Figure R32 b-c**). Relevant discussions have been provided on pages 7-8 in the revised manuscript.

The polarization and power density curves of PEMFC featuring the Pt1-Ru/C anode under H_2-O_2 and H_2-air conditions demonstrate minor degradation after stability testing, as depicted in **Figure R32b** (Figure S34b-c in the revised Supplementary Information), confirming the exceptional stability of the Pt1-Ru/C anode catalyst.

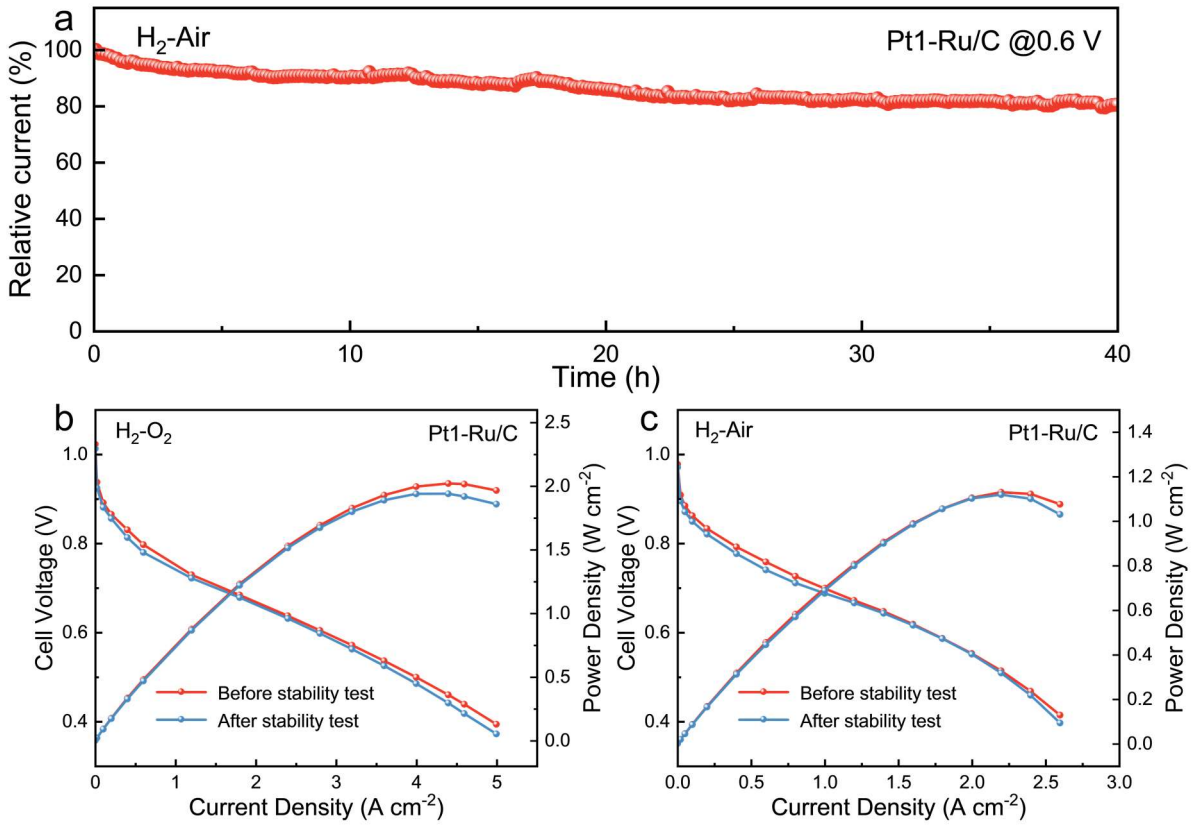

Figure R32. a) Long-term stability tests of the H_2-Air fuel cell at 0.6 V using the Pt1-Ru/C (0.005 mg_{PGM} cm^{-2}) as the anode catalyst. Polarization and power density plots of the PEMFC made with the anode catalyst of Pt1-Ru/C before and after continuous operation at 0.6 V for 40

h under H_2-air condition. b) H_2-O_2 and c) H_2-air. Test conditions: cell temperature at 80 °C, H_2 flow rate at 1 L min^{-1} and O_2/Air flow rate at 2 L min^{-1}, symmetric back pressures at 250 Kpa.

Reviewer #4: This research developed a tandem catalyst composed of ruthenium nanoclusters decorated with platinum single atoms. Additionally, a unique reaction mechanism involving hydrogen spillover was demonstrated through electrochemical tests, operando analysis, and DFT calculations. Especially, the originality of this paper lies in reducing the cost of the PEMFC single cell by drastically minimizing the anode platinum usage. However, additional experiments seem necessary to further explain the performance improvement and enhance its practical applicability. Therefore, this paper requires minor revision for publication in *Nature Communications*.

Comment 1: The author explained the origin of the enhancement in hydrogen oxidation reaction (HOR) kinetics through hydrogen spillover from ruthenium to platinum. Electrochemical analysis and in-situ spectroscopic experiments provided evidence of hydrogen spillover under acidic HOR conditions. Furthermore, ICP analysis showed that the weight percentage of ruthenium is more than eight times that of platinum, and the electrochemical data in Figure 3 indicate that both Pt and Ru sites in the developed catalyst play a significant role in HOR. If hydrogen spillover is favorable and the main reaction pathway, the ratio of ruthenium to platinum and the atomic environment around them would likely have a significant impact. Given this, why does Pt1-Ru/C-2, which has more hydrogen spillover and can more effectively pull up hydrogen strongly bound to Ru, show a lower reaction rate compared to Pt1-Ru/C?

Response to Comment 1: The Pt1-Ru/C catalyst features a coupled structure of Ru nanoclusters and Pt single atoms, where the Pt single atoms are exclusively adsorbed on the surfaces of the Ru nanoclusters. This configuration enables sufficient Pt-Ru interfacial sites for hydrogen spillover effects, despite the Pt/Ru mass ratio being 1:8.

Actually, the catalytic activity of the Pt1-Ru/C-2 catalyst remains comparable to that of Pt1-Ru/C (**Figure R33**). This is attributed to the saturation coverage of Pt atoms on Ru nanoclusters in Pt1-Ru/C, where excess Pt atoms do not participate in the spillover effects with Ru clusters. As depicted in **Figure R33** (Figure S20 in the revised Supplementary Information), the Pt1-Ru/C-2 and Pt1-Ru/C catalysts exhibit nearly identical LSV polarization curves, exchange current densities (j_0), and kinetic current densities (j_k). However, Pt1-Ru/C-2 displays slightly inferior mass-normalized activity ($j_{0,m}$ and $j_{k,m}$) compared with Pt1-Ru/C. This divergence stems from the near-saturation Pt coverage on Ru nanoclusters in Pt1-Ru/C and excess Pt atoms

cannot engage in the hydrogen spillover interactions with Ru nanoclusters. Consequently, these redundant Pt sites contribute negligibly to HOR enhancement, ultimately reducing the mass-normalized activity of Pt1-Ru/C-2 compared with Pt1-Ru/C.

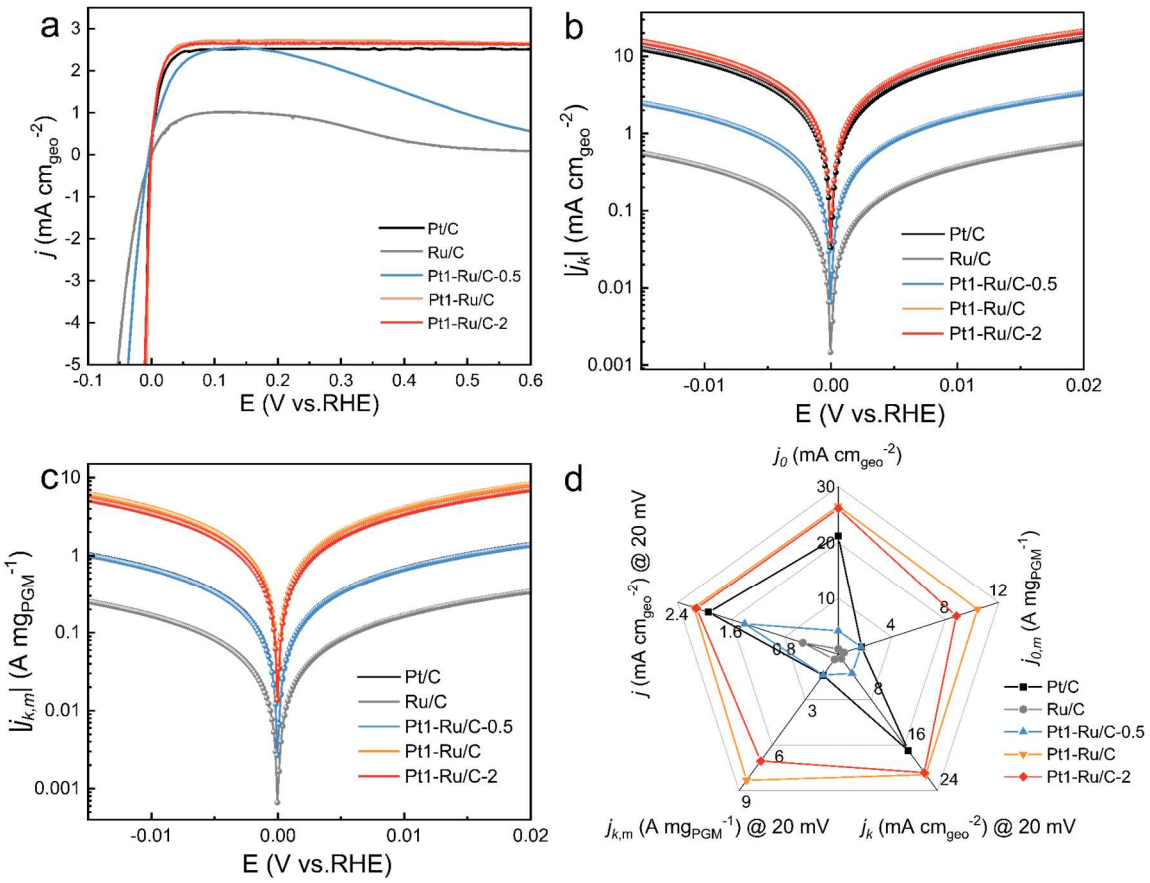

Figure R33. Electrochemical measurement results. a) Geometric area-normalized LSV curves of different catalysts. b) Calculated HOR kinetic current densities (j_k) versus potential plots recorded from (a). c) PGM mass-normalized HOR kinetic current densities (j_k) versus potential plots. d) Comparison of j_k, $j_{k,m}$ (mass-normalized j_k), and j at an overpotential of 20 mV and j_0, $j_{0,m}$ (mass-normalized j_0) of different catalysts.

Comment 2: According to the author's fitting results, Ru exists only as a metallic cluster phase, while Pt has chlorine or oxygen coordination. Why is Pt-Ru coordination not considered? Additionally, if only chlorine coordination is present, an explanation is needed as to why the oxidation state of Ru changes.

Response to Comment 2: We further analyzed the EXAFS results of different samples by employing the continuous Cauchy wavelet transform (CCWT) analysis, revealing distinct Pt-Ru coordination in the Pt1-Ru/C-A samples, whereas such metal-metal bonding is absent in the

non-activated Pt-Ru/C. This phenomenon arises from the electrostatic adsorption of $PtCl_6^{2-}$ precursors on the Ru nanocluster surfaces, wherein the Cl^- ligands create steric hindrance that blocks direct Pt-Ru atomic contact, thereby preventing the formation of Pt-Ru bonds. However, the activation process triggers the structural reconstruction of Pt1-Ru nanoclusters, which simultaneously facilitates chloride removal and induces direct bonding between Pt and Ru atoms in Pt1-Ru/C-A.

As for the changes of Ru oxidation state, it probably arises from the electron transfer between Ru and $PtCl_6^{2-}$, as evidenced the reduced Pt-Cl coordination numbers in the Pt1-Ru/C catalyst (Table S3 in the revised Supplementary Information).

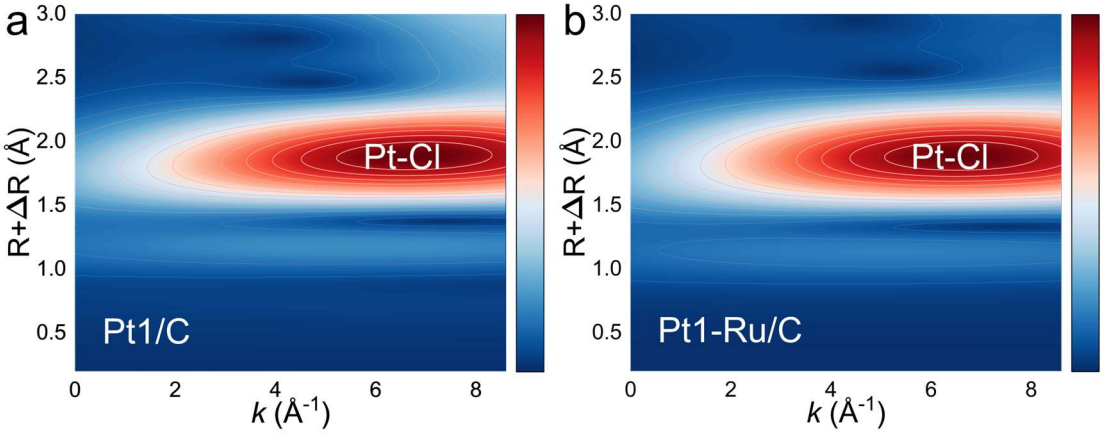

Figure R34. The continuous Cauchy wavelet transform (CCWT) for the k^3-weighted EXAFS signals at the Pt1/C (a) and Pt1-Ru/C (b).

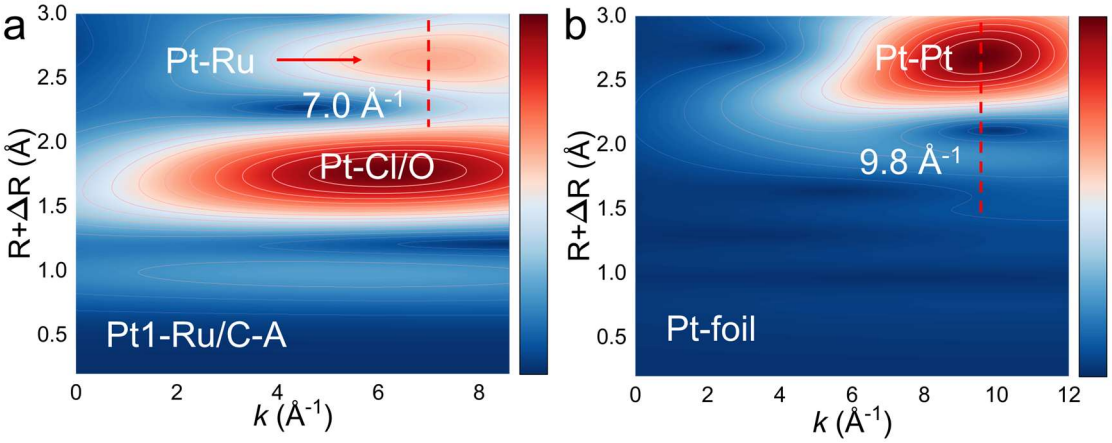

Figure R35. The continuous Cauchy wavelet transform (CCWT) for the k^3-weighted EXAFS signals at the Pt1-Ru/C-A (a) and Pt-foil (b).

Specifically, as shown in the **Figure R34b**, the Pt1-Ru/C sample shows no significant metal-metal coordination. In contrast, the Figure R35a reveals clear evidence of metal-metal

coordination at 2.65 Å for the HOR overpotential-activated Pt1-Ru/C-A sample. The k-space positions of metal-metal coordination in Pt1-Ru/C-A are centered at 7.0 $Å^{-1}$, significantly lower than the 9.8 $Å^{-1}$ position characteristic of Pt-Pt bonds in Pt-foil (**Figure R35b**). The downshift of the central position in k-space indicates the presence of lighter elements in the coordination shell. In our case, it is the emergence of Pt-Ru bonds. Based on the finding, we re-fit the EXAFS spectra of the Pt1-Ru/C-A. The coordination number of the Pt-Ru bonds are determined to be 0.7, as detailed in Figure S10 and Table S3 (in the revised Supplementary Information). Relevant discussions have been provided on pages 4-5 in the revised manuscript.

Comment 3: In Figure 2, Pt1-Ru/C anode HOR catalysts shown high performance of PEMFC under practical H_2-air condition. Additionally, high CO tolerance during HOR of Pt1-Ru/C exhibited as a suitable PEMFC anode material. Authors mentioned that developed materials can be used for automobile power source. Achieving practical high performance PEMFC is necessary not only high power but also long-term durability. So, Authors need to show PEMFC single-cell durability test of developed catalyst with reference Pt/C catalyst.

Response to Comment 3: Thanks. The durability of the PEMFC with the Pt1-Ru/C anode was evaluated through continuous operation at 0.6 V under H_2-air testing condition for 40 h (**Figure R36a**), and the polarization and power density plots of the PEMFC were obtained before and after the continuous operation in both H_2-O_2 and H_2-air conditions (**Figure R36b-c**). Relevant discussions have been provided on pages 7-8 in the revised manuscript.

The polarization and power density curves of PEMFC featuring the Pt1-Ru/C anode under H_2-O_2 and H_2-air conditions demonstrate minor degradation after stability testing, as depicted in **Figure R36b** (Figure S34b-c in the revised Supplementary Information), confirming the exceptional stability of the Pt1-Ru/C anode catalyst.

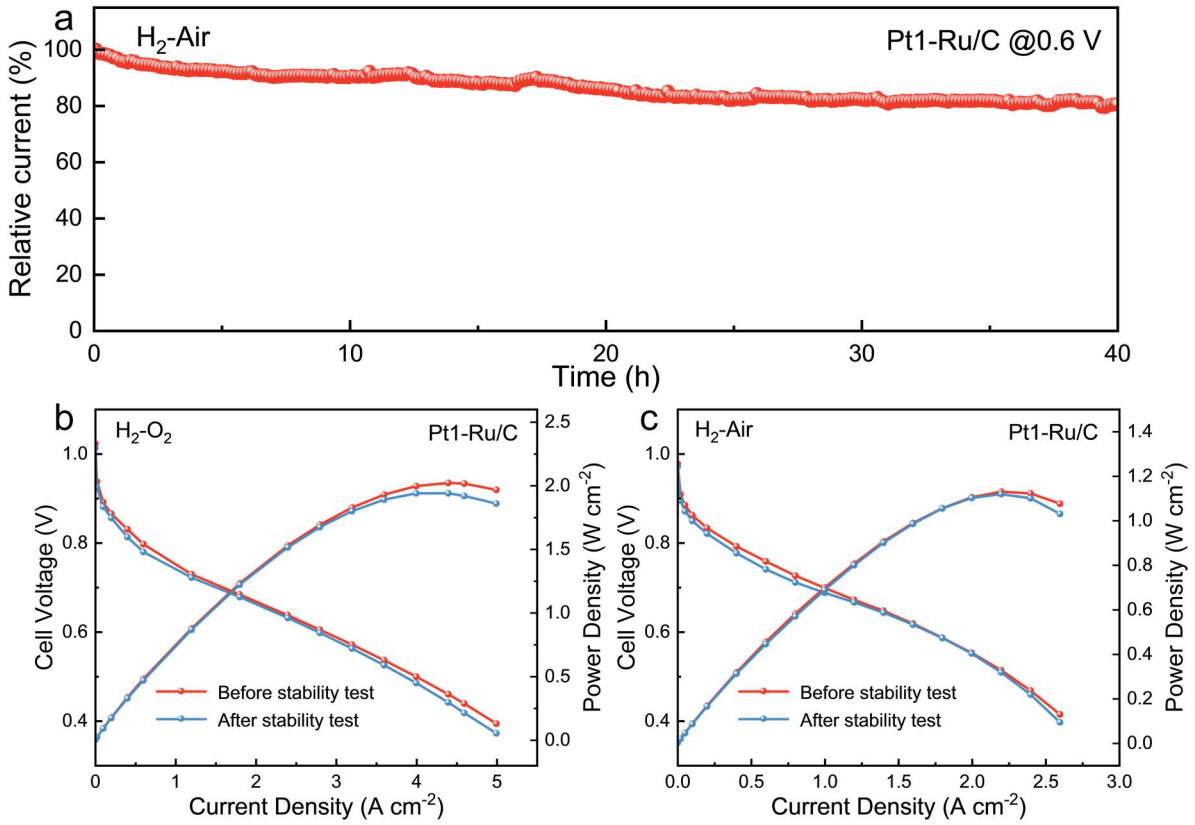

Figure R36. a) Long-term stability tests of the H_2-Air fuel cell at 0.6 V using the Pt1-Ru/C (0.005 mg_{PGM} cm^{-2}) as the anode catalyst. Polarization and power density plots of the PEMFC made with the anode catalyst of Pt1-Ru/C before and after continuous operation at 0.6 V for 40 h under H_2-air condition. b) H_2-O_2 and c) H_2-air. Test conditions: cell temperature at 80 °C, H_2 flow rate at 1 L min^{-1} and O_2/Air flow rate at 2 L min^{-1}, symmetric back pressures at 250 Kpa.

Reviewer #5: The manuscript presents a Pt1-Ru catalyst for efficient HER and HOR. A tandem mechanism in which hydrogen spillover from Ru to Pt site is proposed. The authors performed passivation, KIE, FTIR, and DFT calculations to support their hypothesis. Although the performance of the catalyst is impressive, the active site assignments are not consistent throughout the study, which renders the mechanistic study untrustworthy. The detailed comments are listed below. Based on these inconsistencies presented in the study, I do not recommend the manuscript for publication in Nat. Commun. in its current form.

Comment 1: The EXAFS in Figure 1d and fitting results seem to support that Pt has O/Cl coordination and its oxidation state is 2+ or 4+. However, in the Pt single atom is modeled with Pt adatom on Ru surface, which has no ligand protection and should be of oxidation state 0. This inconsistency with EXAFS characterization results and DFT model decrease the reliability of the proposed tandem mechanism.

Response to Comment 1: Based on the EXAFS analysis, we reconstructed the Pt1-Ru structural model for DFT calculations, as depicted in **Figure R37** (Figure 6 in the revied manuscript), where isolated Pt atoms are coordinated by two oxygen atoms on the Ru surface. The calculated free energy barriers for direct H* desorption from Ru and Pt sites are 0.44 and 0.31 eV, respectively (Figures S45-46 in the revised Supplementary Information). In contrast, the free energy for hydrogen spillover from Ru to Pt single atoms and desorption from Pt single atoms are 0.16 and 0.23 eV, respectively (Figure R37a-b). The decoupled HOR enabled by the hydrogen spillover effect not only reduces the desorption free energy of H* at Ru sites but also lowers the energy barrier of the rate-determining Volmer step. The recalculated results still prove the reliability of the decoupled HOR mechanism.

Relevant discussions have been provided on page 14 in the revised manuscript.

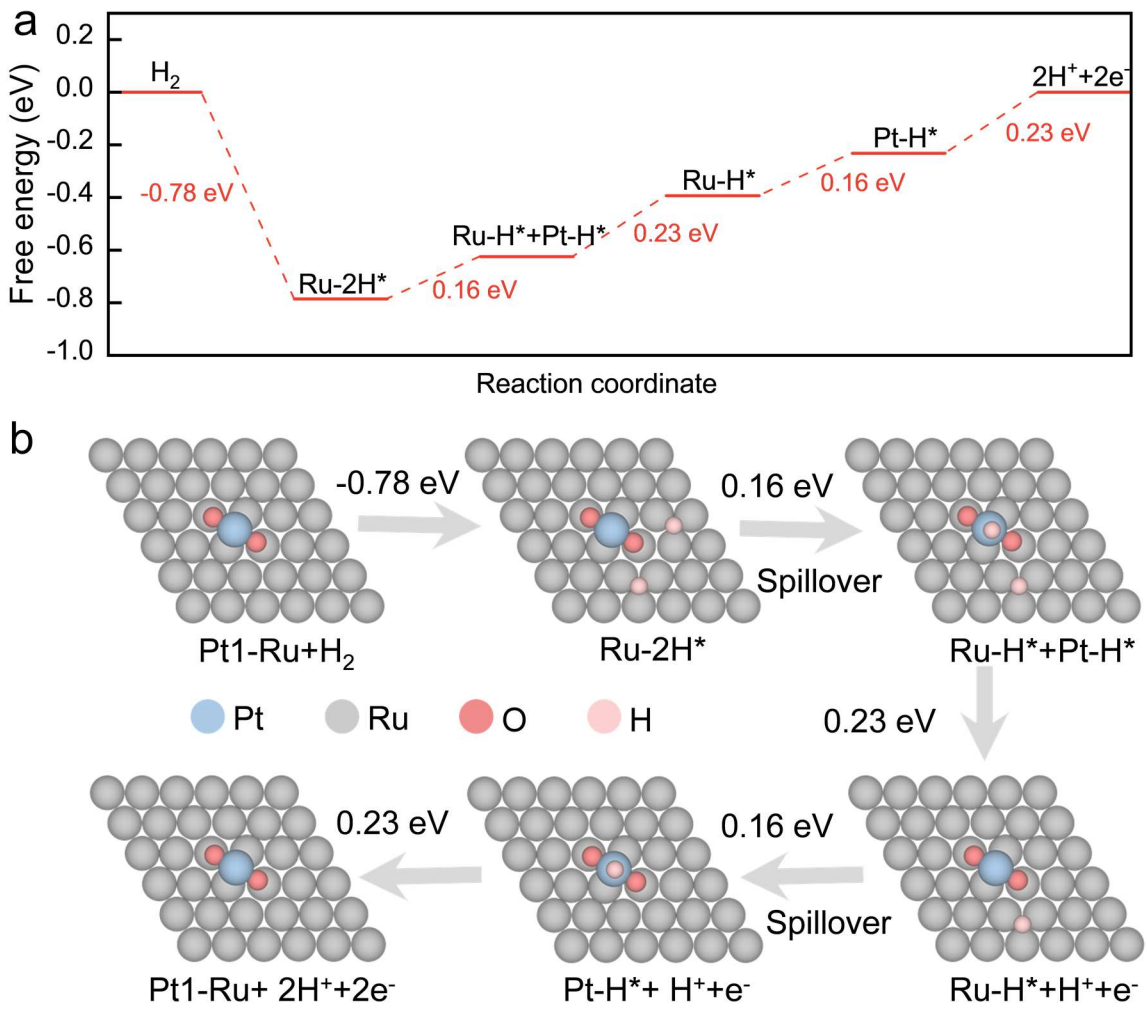

Figure R37. Theoretical calculation investigations. a) Gibbs free energy diagram for HOR on Pt1-Ru. b) Pt1-Ru models and schematic diagrams of the hydrogen spillover process as well as the corresponding free energy of each step.

Comment 2: The working conditions is not taken into account for mechanism proposal and the active site is not clear for HOR/HER. The authors mentioned that Ru starts to be oxidized at 0.1 V, so in the HOR conditions, are Ru metallic or bounded with OH and O? What are the influences of Ru oxidation state on H_2 dissociation reaction? Does it influence the H spillover to Pt? I think these are important points that needed to be further elucidated. The same question also needed to be answered for HER.

Response to Comment 2: The oxidation of Ru at high potentials in acidic media occurs through the formation of Ru-OH bonds, with oxygen species derived from water deprotonation (*CCS Chem.* **2024,** Just Published. DOI: 10.31635/ccschem.024.202404436).

In the Pt1-Ru/C catalyst, the stable limiting current density of Pt1-Ru/C (**Figure R38**) indicates that decorating Ru clusters with Pt single atoms effectively protects Ru sites from poisoning by oxygen-containing species (*Nano Res.* 2024, 17, 6147–6156). Additionally, as depicted in **Figure R39**, Figure S7, and Figure S14 in the revised Supplementary Information, the Ru K-edge XANES and XPS analyses of the Pt1-Ru/C catalyst revealed no significant oxidation behavior of Ru species after activation at 0.1 V, further confirming the robust oxidation resistance of the catalyst.

As for the HER, the hydrogen adsorption on metallic Ru and the hydrogen spillover effect remains unaffected. We measured the Ru 3p XPS spectra (**Figure R40a**) and TEM images of Pt1-Ru/C after activation at -0.1 V for 3 h (**Figure R40b**). The results reveal that Ru retains the metallic state without significant agglomeration.

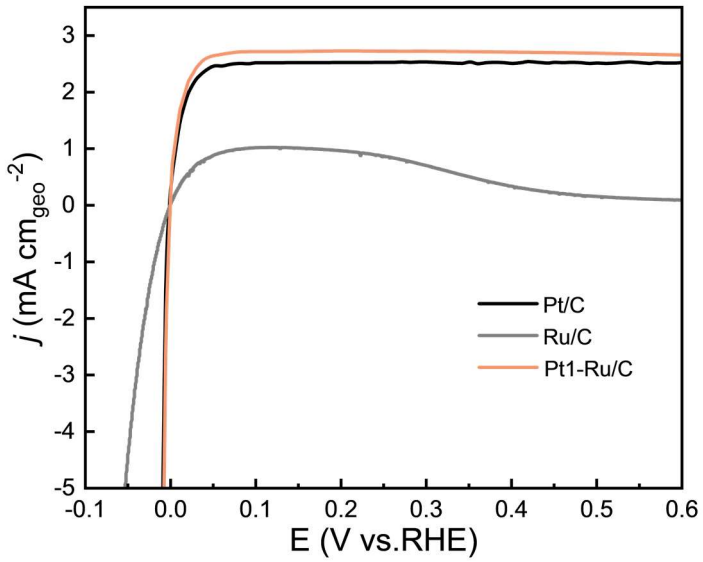

Figure R38. Geometric area-normalized LSV curves of different catalysts.

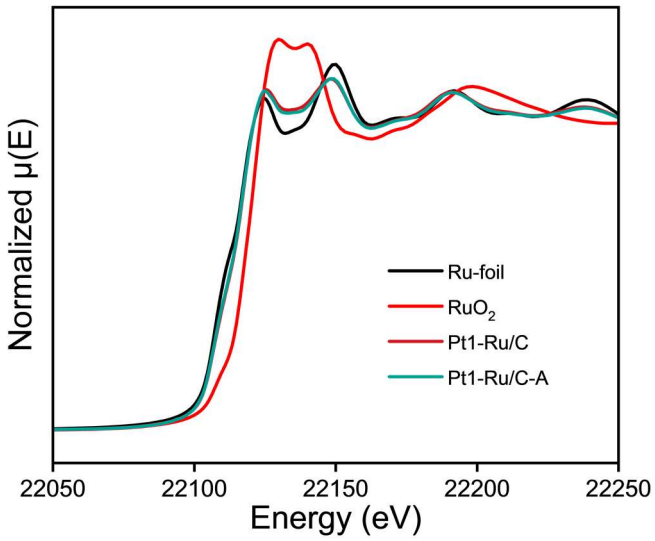

Figure R39. Ru K-edge XANES spectra of Ru-foil, RuO_2, Pt1-Ru/C, and Pt1-Ru/C-A.

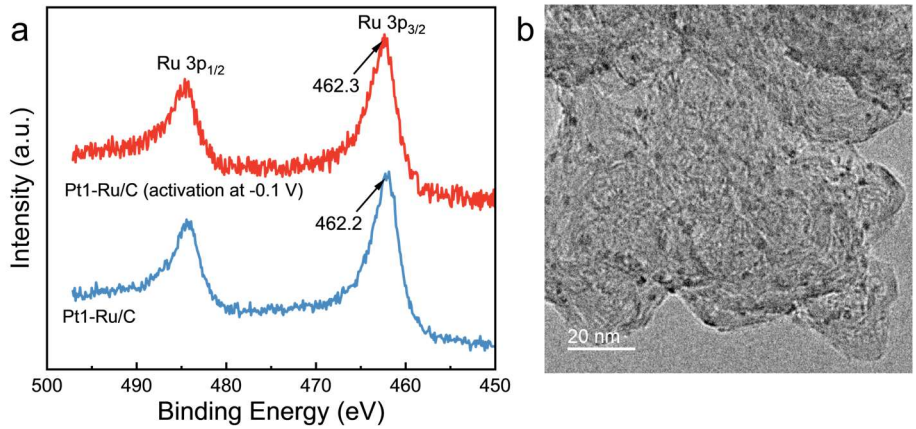

Figure R40. a) Ru 3p X-ray photoelectron spectroscopy (XPS) spectra of Pt1-Ru/C and Pt1-Ru/C (activation at -0.1V). b) TEM image of Pt1-Ru/C (activation at -0.1V).

Comment 3: In HER conditions, Pt1-Ru catalysts is supposed to be reduced. Does it lead to Pt aggregation because of the ligand removal? What the form of Pt and Ru in HER conditions?

Response to Comment 3: Under HER conditions, Pt and Ru persist as oxygen-coordinated single-atom Pt sites and Ru nanoclusters, respectively. A series of *ex situ* characterizations were conducted to monitor structural changes in the catalyst under HER potentials. Following 3-hour activation at -0.1 V overpotential (denoted to as Pt1-Ru/C-A (-0.1 V)), the Pt single atoms exhibited a significant reduction in oxidation state (**Figure R41a**) along with an increased Pt-

O coordination number of 1.8 (**Figure R41b-d**), indicating that Pt is further reduced and converted into oxygen-coordinated single atoms during HER. The observed k-space central position downshift reveals the formation of Pt-Ru bonds (**Figure R41c**). Post-activation characterization in **Figure R41e** demonstrates well-maintained atomic dispersion of Pt species on Ru nanoclusters after -0.1 V treatment. Additionally, The Ru 3p XPS analysis (**Figure R40**) confirms the persistent metallic state of Ru throughout HER operation.

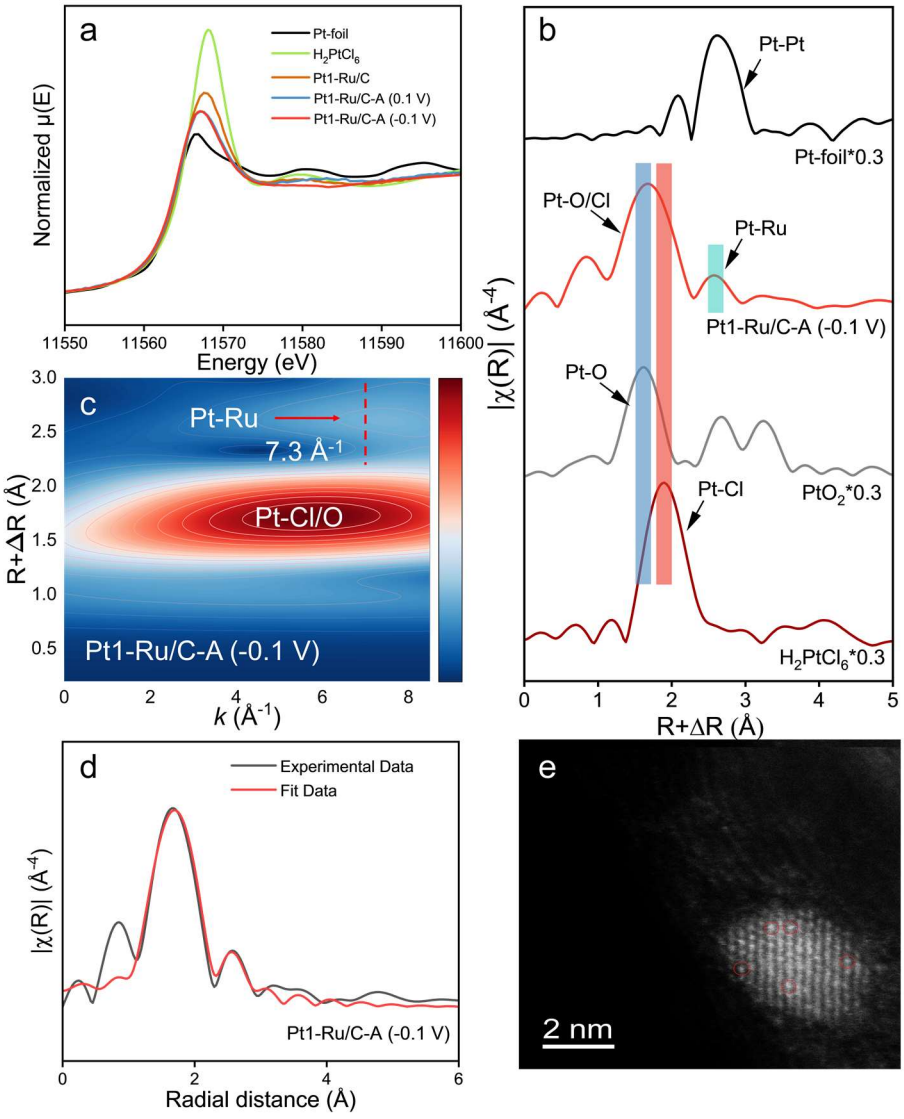

Figure R41. a) Pt L_3-edge XANES spectra of Pt-foil, PtO_2, H_2PtCl_6, Pt1-Ru/, Pt1-Ru/C-A, and Pt1-Ru/C-A (-0.1 V), b) Pt L_3-edge EXAFS spectra of Pt-foil, PtO_2, H_2PtCl_6, and Pt1-Ru/C-A (-0.1 V), c) the corresponding Cauchy Wavelet Transform (CCWT) for the k^3-weighted EXAFS signals at the Pt1-Ru/C-A (-0.1 V), d) the Pt L_3-edge fitted EXAFS spectra of Pt1-Ru/C-A (-0.1 V), and e) HAADF-STEM images of Pt1-Ru/C after activation at an overpotential of 0.1 V for 3 h.

Comment 4: The noise to signal ratio of the FTIR data in Figure 5 is really bad. I don't think it gives out reliable support for the proposed mechanism. And, H* binds to the hollow site on Ru instead of top site.

Response to Comment 4: While the signal-to-noise ratio in Figure 5 appears not good, discernible trends in Pt-H and Ru-H peak evolution remain observable. In addition to the *in situ* synchrotron ATR-FTIR characterization for the hydrogen spillover mechanism, we provide a series of electrochemical evidences to support this phenomenon, including scan-rate-dependent H* desorption peak analysis (Figure 4a-b), HER Tafel slope characterization (Figure 4c-d), pH-dependent HER activity measurements (Figure 4e), isotope effect studies (Figure 4f-h), H_2 temperature-programmed desorption (H_2-TPD, Figure 4i), and *in situ* electrochemical impedance spectroscopy (*in situ* EIS, Figures S37-S39 in the revised Supplementary Information). These experimental findings consistently support the *in situ* synchrotron ATR-FTIR observations, collectively demonstrating the occurrence of hydrogen spillover. Therefore, it is safe to obtain the proposed mechanism in this study.

Moreover, as for the adsorption of H* on Ru, it has been reported that the Ru–H vibrational peak observed near 1900 cm^{-1} in the *in situ* synchrotron ATR-FTIR spectroscopy should be ascribed to the hydrogen adsorbed at the top site of Ru (*Nat. Catal*. 2021, 4, 711–718). In infrared experiments, the detected signals primarily originate from infrared-active vibration modes. Adsorption at top sites typically induces significant changes in dipole moments, thereby enhancing the detectability of the associated vibrational mode — even though these configurations are not the most thermodynamically stable. Therefore, although H is more inclined toward the hollow site at equilibrium based on DFT calculation (*ACS Catal.* 2018, 8, 7, 5714–5720), the observed Ru–H vibrational peak observed near 1900 cm^{-1} should be ascribed to hydrogen adsorbed at the top site of Ru.

Comment 5: in DFT calculations of hydrogen dissolution, I found that the H_2 dissociates into a surface H* and a H in vacuum as seen in Figure 6b. The model is not realistic.

Response to Comment 5: Thanks. We have corrected the errors in the revised manuscript, and the correct computational procedures are now clearly presented in **Figure R37** (Figure 6 in the revised manuscript).

Comment 6: in Figure 1d caption, it should be EXAFS not XANES.

Response to Comment 6: Thanks. We have corrected this issue in the revised manuscript.

Responses to Reviewers

Reviewer #1: The authors have answered all of the questions. It can be considered as a publication in the present form.

Response: We sincerely thank your invaluable comments and suggestions which are critical for improving the manuscript quality.

Reviewer #2: The authors have responded to all of my comments. I am satisfied with the current version and believe it is suitable for publication.

Response: We sincerely thank your invaluable comments and suggestions which are critical for improving the manuscript quality.

Reviewer #3: The authors have addressed the points and concerns raised by the reviewers, and the revised manuscript appears suitable for publication.

Response: We sincerely thank your invaluable comments and suggestions which are critical for improving the manuscript quality.

Reviewer #4: The authors have adequately addressed all reviewer concerns. In response to my primary comment, they provided a clear explanation regarding the hydrogen spillover effect and its saturation behavior, supporting their claim with comparative electrochemical data (Figure R33). They convincingly argue that the slightly lower mass-normalized activity of Pt_1-Ru/C-2 stems from the excess Pt atoms not contributing to spillover interactions due to surface saturation. This mechanistic rationale is supported by both experimental trends and structural considerations.

Furthermore, the authors responded rigorously to the EXAFS coordination concerns, incorporating continuous Cauchy wavelet transform (CCWT) analysis to clarify the emergence of Pt–Ru bonding post-activation. The identification of metal–metal coordination at ~2.65 Å and corresponding k-space shifts substantiates their interpretation. Additionally, their explanation of oxidation state changes via electron transfer from Ru to $PtCl_6^{2-}$ is consistent with the spectroscopic data.

Finally, they supplemented the manuscript with a 40-hour PEMFC durability test under H_2-air conditions (Figure R36), demonstrating minimal degradation and reinforcing the catalyst's

practical viability. Overall, the revised manuscript demonstrates a high level of technical rigor, originality, and relevance to the field of low-PGM PEMFCs. I consider it suitable for publication in Nature Communications after minor revision.

Response: We sincerely thank your invaluable comments and suggestions which are critical for improving the manuscript quality.

Reviewer #5: The computational model has been improved in the revised manuscript. However, the Figure 6 in the revised manuscript seems still not supporting the H spillover mechanism since uphill free energy landscape for H* migrating from Ru to Pt sites are obtained. So basically, H* spillover is not thermodynamically supported. The author needs to further elucidate why Ru could accelerate the HOR. To the best of my knowledge, Pt itself could readily dissociate H_2 into H*, would Ru be necessary to facilitate H-H bond breaking? And, as H* adsorbed strongly on Ru, it is expected that H* may not easily migrate to Pt. These points need to be further elucidated.

Response: First, thermal disturbance energy allows H to transfer to Pt by crossing a small energy barrier. Specifically, hydrogen spillover is a diffusion process, and the diffusion coefficient (D) follows the Arrhenius equation:

$$D = D_0 e^{(-\frac{E_a}{k_B T})}$$

where E_a is the diffusion energy barrier, and $k_B T$ represents the energy provided by thermal disturbance. As can be seen from the equation, diffusion behavior will persist when the temperature is above absolute zero. Therefore, thermal disturbance supplies the energy for facilitating non-spontaneous hydrogen spillover processes (*Angew. Chem. Int. Ed.* 2023, 62, e202312796; *Nat Commun*, 2022, **13**, 1189; *Nat Commun*, 2021, **12**, 3502).

Second, the high H* coverage on the Ru surface can provide an extra driving force for hydrogen spillover toward Pt (*ACS Catal.* 2019, 9, 7876; *Int. J. Hydrogen Energy,* 2018, 43, 5576; *Phys. Chem. Chem. Phys.*, 2015,17, 19446). Specifically, H* continuously accumulates on Ru during the HOR process, creating a significant concentration gradient of H* between the Ru and Pt surfaces. The low H* coverage on Pt sites strongly drives the hydrogen spillover toward Pt.

Therefore, the apparent driving force and actual rate of hydrogen spillover are significantly enhanced by the H* concentration gradient between the Ru and Pt surfaces.

More importantly, once H* transfers to a Pt site, it rapidly undergoes desorption at the anode potential. This subsequent desorption step functions as a "pumping mechanism," continuously consuming H* on Pt sites and thereby maintaining extremely low H* coverage on Pt. This process ensures the continuous occurrence of hydrogen spillover.

In this study, Ru is not employed to accelerate H–H bond dissociation on Pt. Instead, additional Pt sites are required to facilitate the desorption of H* adsorbed on Ru.

Ru sites exhibit strong H* adsorption capability. Failure of H desorption and migration promptly from Ru sites can poison these active centers, thereby blocking subsequent H_2 adsorption and dissociation. Therefore, this study leverages the hydrogen spillover effect to drive H* transfer from Ru to Pt, followed by its desorption. This approach not only addresses the issue of excessive H* adsorption on Ru but also further reduces the cost of PEMFC anode catalysts.

The enhanced HOR kinetics is attributed to the decoupled HOR process. This mechanism replaces the 0.44 eV barrier for Ru-H desorption (Figure S45) with two distinct processes: hydrogen spillover and Pt-H desorption. As a result, compared with the conventional HOR systems, this approach achieves a lower barrier for the rate-determining step, thereby reducing the reaction overpotential.

Review comments

Minor Revision

This research developed a tandem catalyst composed of ruthenium nanoclusters decorated with platinum single atoms. Additionally, a unique reaction mechanism involving hydrogen spillover was demonstrated through electrochemical tests, operando analysis, and DFT calculations. Especially, the originality of this paper lies in reducing the cost of the PEMFC single cell by drastically minimizing the anode platinum usage. However, additional experiments seem necessary to further explain the performance improvement and enhance its practical applicability. Therefore, this paper requires minor revision for publication in *Nature Communications*.

1. The author explained the origin of the enhancement in hydrogen oxidation reaction (HOR) kinetics through hydrogen spillover from ruthenium to platinum. Electrochemical analysis and in-situ spectroscopic experiments provided evidence of hydrogen spillover under acidic HOR conditions. Furthermore, ICP analysis showed that the weight percentage of ruthenium is more than eight times that of platinum, and the electrochemical data in Figure 3 indicate that both Pt and Ru sites in the developed catalyst play a significant role in HOR. If hydrogen spillover is favorable and the main reaction pathway, the ratio of ruthenium to platinum and the atomic environment around them would likely have a significant impact. Given this, why does Pt1-Ru/C-2, which has more hydrogen spillover and can more effectively pull up hydrogen strongly bound to Ru, show a lower reaction rate compared to Pt_1-Ru/C?
2. According to the author's fitting results, Ru exists only as a metallic cluster phase, while Pt has chlorine or oxygen coordination. Why is Pt-Ru coordination not considered? Additionally, if only chlorine coordination is present, an explanation is needed as to why the oxidation state of Ru changes.
3. In Figure 2, Pt1-Ru/C anode HOR catalysts shown high performance of PEMFC under practical H2-air condition. Additionally, high CO tolerance during HOR of Pt1-Ru/C exhibited as a suitable PEMFC anode material. Authors mentioned that developed materials can be used for automobile power source. Achieving practical high performance PEMFC is necessary not only high power but also long-term durability. So, Authors need to show PEMFC single-cell durability test of developed catalyst with reference Pt/C catalyst.